Liberation from fibrogenesis or tumorigenesis via cellular senescence by a novel small molecule

Moon Kee Meang[1*], Saesbyeol Kim[1*], and Byung-Soo Youn[1#]

[1]Osteoneurogen. Inc, Seoul, 08501, Republic of Korea,

Running title: Exodus from uncontrolled proliferative diseases

*Those who contributed to these works equally

[#]Corresponding author, E-mail address: byung4jc@gmail.com

#411, 128, Gasan digital 1-ro,
Geumcheon-gu, Seoul, 08507
Republic of Korea
Tel) 822- 6267-2739
Fax) 822-6267-2740
Cell)82-2- 10-2793-2737

Abstracts

Uncontrolled proliferative diseases such as fibrosis or cancers are fatal human disorders. Previously, we found that a chromone-scaffold derivative called ONG41008 had a strong anti-fibrotic effect on *in vitro* fibrogenesis as well as in a murine lung fibrosis model. It later occurred to our attention that while ONG41008 remarkably attenuated proliferation of diseased human lung myofibroblasts (DHLF), resulting in replicative senescence (RS) typified by cell flatness, normal human lung fibroblasts were not affected. Video demonstration revealed that RS was evident within 48hr after ONG41008 treatment. No ONG41008 affected activated caspase 3 and mitochondrial membrane potential in DHLF. An interactome study suggested that metabolic shift, chromatin remodeling, or cell cycle control may be required for the RS. This observation prompted us to be engaged in cellular senescence of tumor cells. Clearly, senescent cells were conspicuously but temporarily observed in A549, adenocarcinomic human alveolar epithelial cells, giving us confidence that dysregulated cell proliferation could be a common underlying principle conserved in both DHLF and A549. An early phase of stimulation of A549 by ONG41008 led to RS followed by multinucleation (MNC), which has been known to be oncogene-induced senescence (OIS). MNC was immediately followed by apoptosis. Concomitant with massive upregulation of p16 and translocation to the nuclei, complete cell death of the remaining A549 occurred. Induction and nuclear translocation of p21was also noted in both A549 and DHLF stimulated with ONG41008. No induction of TP53 was seen but phosphorylation of TP53 was substantially increased in A549. Both immunocytochemistry and western blots corroborated these common senescent imaging features. With comparative analyses, it is clear that ONG41008 exhibited much lesser toxicity on normal human lung fibroblast than SAHA (suberoylanilide hydroxamic

acid) and Nintedanib. ONG41008 predominantly induced G2/M arrest in A549. Clear formation of MNC was noted in aggressive cancer cell lines involving MCF7 and PC3. A massive increase in NAD/NADH ratio was made by ONG41008, likely impacting mitochondrial function. This may explain how ONG41008 initiated OIS via ROS production in the recovered mitochondria. On the contrary, SAHA did not affect NAD/NADH ratio.

Taken together, all these studies strongly suggest that ONG41008 is a potent inducer of RS or OIS, resulting in cessation of cell cycle are at G2/M cell cycle stages and/or systemic cell death. To our best knowledge, the liberation of uncontrolled proliferative cells from fibrogenesis or tumorigenesis by a small molecule *in vitro* is an unprecedented case. ONG41008 could be a potential and safe drug for a broad range of fibrotic diseases or tumorigenic diseases.

Funding: an Osteoneurogen intramural fund

Key words

Anti-proliferation, Cellular senescence, Fibrosis, Cancer, and Small molecule

Introduction

Uncontrolled cell cycle progression has been well appreciated in terms of close association with rise of fibrosis or cancer [1]. Cells need to tightly regulate cell cycle entry and exit [2], otherwise leading to disastrous consequences involving tumorigenesis [3]. Although targeting cell cycle progression by small molecules has been considered an intriguing cancer modality undesirable medical risks such as systemic inhibition of stem cell differentiation or aggravation of homeostatic immunity may happen [4]. In this regard, natural drug scaffolds such as chromone-scaffold (CS) largely discovered in flavones or isoflavones may be able to provide a great deal of medical benefits to these proliferative diseases because these natural products have been largely proven to be safe and to give rise to unexpected desirable effects on suppression of uncontrolled proliferation shown by pathogenic myofibroblasts or aggressive tumor cells [5]. Metastasis plays a conclusive role in cessation of onset of cancer and has been a cancer target [6]. And it has been increasingly clear that metabolic regulation is closely coupled to cell cycle in cancer cells. Exclusive dependence of tumor cell growth on aerobic glycolysis, alternatively called lactate fermentation, has been well established [7]. Similarly, myofibroblasts utilize aerobic glycolysis and tend to generate hypoxia, playing a central role in the initiation and perpetuation of fibrosis [8].

Flavones are members of the polyphenol family, a group of over 10,000 compounds have been exclusively found in the plant kingdom [9]. In general, these phytochemicals protect plants from radiation damage [10]. Due to their anti-oxidant or anti-inflammatory potentials, flavones have long been used to treat inflammatory diseases such as arthritis and asthma [11]. Chromone, 1,4-benzopyrone-4-one, is a central chemical scaffold constituting flavones and isoflavones [12]. We recently reported that eupatilin, a CS-containing compound from an

Artemisia species and its analog called ONG41008 substantially inhibited fibrogenesis *in vitro* and fibrosis *in vivo* via actin depolymerization followed by dismantling latent TGFβ complex (LTC). This resulted in inhibition of epithelial-mesenchymal-transition (EMT) [13]. Here, we show that ONG41008 is a potent inducer of replicative senescence (RS) in pathogenic myofibroblasts and oncogene-induced senescence (OIS) in several human aggressive cancer cell lines, respectively, thereby being escaped from fibrogenesis and tumorigenesis. These therapeutic capabilities of ONG41008 in terms of anti-proliferation may open a door as a powerful new therapeutic modality as regenerative medicine for treating fibrosis as well as cancer.

Results

ONG41008-treated DHLF exhibited cell growth arrest, leading to replicative senescence (RS).

Disease human lung fibroblasts from IPF patients (DHLF) are αSMA+ pathogenic myofibroblasts also expressing an array of muscular collages. We sought to identify differential therapeutic modes by two first-in class idiopathy pulmonary fibrosis (IPF) drugs, nintedanib and pirfenidone as compared to that of ONG41008. Due to a drug-repurposing from cancer to IPF, nintedanib has been well appreciated for induction of cellular toxicity whereas pirfenidone is known to be hepatotoxic and seems to indirectly modulates immune cells function, thereby producing lesser active TGFβ [14] [15]. We lately reported that ONG41008 was a TGFβ-biogenesis inhibitor, immediately being capable of establishing cessation of TGFR signaling, resulting in reprogramming EMT to MET [13]. As shown in Figure 1A, nintedanib was able to induce a robust cell death in 24hr and a longer exposure in 48hr virtually killed all DHLF. IC_{50} was 10.17μM at 72hr. Pirfenidone remained unresponsive in terms of cell survival. Interestingly, ONG41008 marginally affected cell survival and its maximal survival rate remained over 60% regardless of increase in ONG41008 concentrations, resulting in no IC_{50} value. This strongly indicate that a systemic growth arrest may largely occur at the ONG41008 treatment of DHLF. Our previous 14 Day non-GLP Tox. study suggests that ONG41008 was essentially non-toxic to mice and rats and no perturbed pathologic features were observed (data not shown). As a control experiment, normal human lung fibroblasts (NHLF) were similarly treated as in the case of DHLF. Surprisingly, while nintedanib gave rise to a drastically low cell survival rate and pirfenidone remained unresponsive as in the case of DHLF. However, ONG41008 didn't essentially affect NHLF, not allowing us to calculate IC_{50}.

But, the IC_{50} of nintedanib was around 30μM (Figure 1B). The susceptibility of DHLF to nintedanib in terms of apoptosis was more enhanced than that of NHLF.

In order to rule out involvement of apoptosis in ONG41008-mediated growth arrest in DHLF, three apoptotic means were exploited; 1) activated Caspase3 assay, 2) mitochondrial membrane potential (MTMP), and 3) LDH cytotoxicity assay. FCCP (trifluoromethoxy carbonylcyanide phenylhydrazone) was used as a control for MTMP. As shown in Figure 2A, 2B, and 2C, only nintedanib was able to cause a remarkable apoptosis, giving rise to their respective IC_{50} or EC_{50}, suggesting that the systemic growth arrest induced by ONG41008 was not a consequence of apoptosis and would rather be related to cellular senescence. A hallmark of RS is cell flatness [16]. We previously found that GATA6 plays an important role in perpetuating EMT in DHLF [13]. We assumed that expression of GATA6 would discontinue in the absence of TGFβ but in the presence of ONG41008. A RS model was set up with time lapses microscopy along with increasing ONG41008 concentrations. As shown in Figure 3A, GATA6 expression was consistently seen in the entire RS setting, which remains to be further elucidated. RS was generated at 5μM ONG41008 and became more evident at 10μM. The maximal extent of the RS occurred at 20μM. DHLF in the absence of ONG41008 remained unchanging. This study singled out a conclusion that ONG41008 was a potent inducer of cellular senescence, namely RS, in DHLF. Moreover, two sets of video demonstration clearly showed that RS was evident in the presence of 10μM ONG41008 (Supplementary Video Imaging I at high cell density and II at low cell density). An RNA-seq analysis was done, giving rise to a nuclear interactome as shown in Figure 3B. EGR1 (Early Growth Response 1) was a priming protein, which interacted with an array of proteome involving CDC45 (Cell Division Cycle 45), Transforming Acidic Coiled-Coil Containing Protein 3 (TACC3), or Cyclin

Dependent Kinase 1 (CDK1), which play pivotal roles in onset of nuclear events in cell differentiation, DNA replication, cell cycle control or cellular senescence [17] [18] [19] [20]. We also discovered that unique transcriptomes were also responsible for driving replicative senescence. RNA-seq analysis was again conducted to compare difference in gene expression between DHLF and 10μM ONG41008-treated DHLF. Upregulated genes were sorted out by p-values. As shown in Supplementary Figure 1 and 2, three interactomes seemed to be working cooperatively for being led to RS; the first one was metabolic interactome typified by pyruvate dehydrogenase kinase (PDK)1, the second one was actin biogenesis, and the last one was related to histone modification, DNA replication, and generation of a muscle-neuron signature whereby the DHLF expression signature could be transiently going through to the RS. The reason being generation of a muscle-neuron signature remains to further explored. Interestingly, vast majority of top-ranked genes affected by ONG41008 were soluble factors or receptors (Supplementary Table I). We imagined that prior to euchromatin formation driving RS expression of this array of cytokines or interaction with cognate-receptors might happen for priming cellular senescence.

ONG41008-mediated RS may be required for participation of TP53, p21 and p16 in DHLF

It has been appreciated that several tumor suppressor proteins are responsible for cessation of cell cycle progress [21]. TP53 undergoes phosphorylation and is mainly coupled to p21 or p16, leading to cell cycle inhibition. As shown in Figure 4A, TP 53 was not induced but rapidly translocated to the nucleus 1hr after 1μM ONG41008 treatment. The same held true that p21 in DHLF treated with 1~10μM ONG41008 was upregulated and translocated to the

nuclei (Figure 4B). With respect to p16, it was also upregulated and translocated to the perinuclear zone and the nuclei (Figure 4C). It has been well documented that the cooperative works between TP53, p21 and p16 plays pivotal roles in cell cycle control.

Cellular senescence-mediated apoptosis of A549 by ONG41008

Pathogenic myofibroblasts and tumor cells are in common in many ways; first, aerobic glycolysis is the major catabolism of glucose. Second, uncontrolled cell division occurs. Third, immune escape is a major cause for perpetuation of their existence. The observation that DHLF were rapidly converted to RS by ONG41008 prompted us to see if cancer cells would similarly behave. Cellular senescence was established in A549 with the treatment of 10μM ONG41008 for 24hr, 48hr or 72hr, and immunohistochemistry was conducted enabling us to see morphological change, namely cell flatness [22]. As seen in Figure 5A, flat cell morphology was evident in A549 treated with ONG41008 for 24hr and multinucleated A549 began to appear (Figure 5A and 5B). It has been appreciated that multinucleation of cancer cells is caused by called oncogene-induced senescence (OIS) [23]. Akt1 activation has been detected in A549 [24]. In fact, our ICC data shows that the phosphorylated-Akt1existed in A549 and its levels were augmented in proportional to increasing concentrations of ONG41008 (Supplementary Figure 3). The greatest number of multinucleated A549 was observed at 48hr (Figure 5B), after which the number was significantly reduced (Figure 5C). These studies suggest that ONG41008 was a potent inducer of OIS [25].

Taken together, ONG41008 was able to induce OIS in A549 such that ONG41008-exposed A549 underwent a systemic apoptosis.

Phosphorylation of TP53 and nuclear translocation of phosphorylated TP53, p21, and p16 rapidly occurred prior to the OIS of A549 stimulated with ONG41008

As in the case of induction of RS shown in DHLF we further explored changes of TP53, p21, and p16, which are able to induce OIS in A549. As shown in Figure 6A and 6B, while TP53 protein expression remained unchanging but its nuclear location could be seen at 1μM ONG4008, p21 was upregulated and similarly nuclear localized. p16 was upregulated in proportional to varying concentrations of ONG41008 and was nuclear localized as well as distributed at the perinuclear zones (Figure 6C). We discovered that cell morphology became more homogenous at 72hr after ONG41008 treatment than that of 24hr-long ONG41008 treatment, which may reflect elimination of multinucleated A549. And a maximal translocation of p16 to the nuclei seemed to be completed at 72hr. These p16-satutated A549 would be supposed to undergo apoptosis (Figure 6D and Figure 7B). Since phosphorylation of TP53 is known to be essential for its capability of regulating cell cycle arrest [26], we conducted western blot analysis by using a phospho-specific TP53 antibody. Increase in the concentrations of ONG41008 was proportional to degree of phosphorylation of TP53 (Figure 7A) and total amounts of TP53 remained same. We also noticed that both p21 and p16 were induced in a concentration-dependent manner, which corroborated the results of ICC (Figure 6A, 6B, and 6C). Respective molecular positioning was denoted by yellow circles. We continued to stimulate A549 in the presence of both TGFβ to make A549 more proliferative in conjunction with ONG41008. It was observed that a significant fraction of A549 died off from 6 days and complete cell death occurred at 15 days whereas control A549 remained vibrant (Figure 7B). While blue circles represented control A549 growth, blue and red circles

denoted control A549 and ONG41008-treated A549, respectively. All cells exposed to 10μM ONG41008 seemed to receive apoptotic signals during 72hr.

In addition to A549, a human triple negative breast cancer cell lines called MCF7 and PANC1, a human pancreatic cancer cell line, were brought into focus. These cells and A549 were stimulated with ONG41008 for 48hr and ICC were conducted. All three cancer cell lines showed robust cellular senescence as shown in Figure 8. MNC were denoted by white circles and presumable mitosis was represented by green circles in a fraction of A549. MNC were not formed in PANC1. Even longer exposure to ONG41008 did not increase is MNC, suggesting that cancer cellular origins may affect MNC. Additionally, a human aggressive prostate cancer cell line, PC3, also exhibited robust formation of MNC as shown in Supplementary Figure 4.

Taken together, ONG41008 was able to induce cellular senescence in cancer cells, most likely being OIS, leading to apoptosis.

Comparison of anti-cancer capabilities between ONG41008 and SAHA

MOA (mode of action) of ONG41008 to eliminate cancer cells seems to be induction of OIS. There are numerous anti-cancer drugs targeted to cell cycle control, DNA replication, or chromatin remodeling, etc. We explored how cellular survival rate and mitochondrial membrane potential were affected by these drugs. We decided to compare between ONG41008 and SAHA (suberoylanilide hydroxamic acid), a reversible pan-histone deacetylase (HDAC) inhibitor, because effect of ONG41008 on cell cycle regulation and that of SAHA on chromatin remodeling seemed to be inter-related to cell cycle division control as well. It should be noted that an important nod in the A549-ONG41008 was HIST1H4K (H4 Clustered Histone 12)

involved in DNA replication and DNA repair (Supplementary Figure 5). As shown in Figure 9A, while substantial attenuation of cell survival by SAHA rapidly occurred at 24hr and seemed to reach a maximum at 72hr via MTMP assay, an inhibitory effect by ONG41008 began at 48hr and continued to be increased to 4 days till all cells were eliminated. The cell killing kinetics made sense in that initiation of OIS by ONG41008 begin at 48hr and continued to be increased till 72hr based upon our ICC data as seen in Figure 5. IC_{50} showed around 20-fold differences. These data suggest that ONG41008-mediated apoptosis was a consequence of induction of OIS whereas SAHA exhibited a rapid cell death due to its HDAC inhibitory effect on a broad range of chromatin remodeling processes, likely a reason being many undesirable effects associated with SAHA. The extent of apoptotic capacity and time duration by ONG41008 in A549 was distinguished from those of SAHA or presumably other anti-cancer drugs as well. In order to ascertain whether ONG41008, SAHA and Nintedanib, an originally designed anti-cancer drug, differentially affected NHLF a set of CCK-8 or MTMP assays were conducted. As shown in 9A, it is clear that while both SAHA and Nintedanib exhibited tremendous toxic effects on NHLF ONG41008 did not give rise to cell toxicity. Furthermore, while SAHA and Nintedanib exhibited robust apoptotic capacities measured by MTMP, Caspase3, and LDH ONG4108 did not exert noticeable degree of apoptosis (Figure 9C, 9D, and 9E).

Cell cycle arrest at G2/M and massive induction of NAD/NADH ratio in A549 by ONG41008

Involvement of TP53, p16, or p21 strongly indicates that ONG41008 played an important role in cell cycle control. Cell cycle analysis using PI staining was conducted at 24hr

and 48hr after ONG41008 treatment of A549. It was clear that ONG41008 predominantly induced G2/M stage. At 50μM, G0/G1 was slightly affected (Figure 10A). Metabolic regulation has been thought to be a key driver for controlling cell cycle regulation or apoptosis [27]. It has been well appreciated that NAD/NADH ratio plays a central role in regulating energy metabolism including glycolysis and TCA cycle and tremendously affects mitochondrial functions such as pathogenesis or ageing [28]. We hypothesized whether ONG41008 could influence NAD/NADH ratio since the hitherto observation of ONG41008 capability of sensing intracellular microenvironments in terms of distinguishing normal cells from uncontrolled proliferative cells like tumor cells or pathogenic myofibroblasts gave us an impetus to explore this possibility. When A549 were stimulated with ONG41008 massive induction of NAD/NADH ratio occurred (Figure 10B). However, SAHA did not affect it. A549 per se, NAD/NADA ratio exhibited minus value, suggesting that A548 may exclusively utilize aerobic glycolysis.

An A549-ONG41008 interactome

Fas may be a central nod, which was the death-domain containing cell surface receptor in OIS-mediated apoptosis in A549 (Figure 10). As an additional evidence supporting that systematic apoptosis could be initiated from additional nodes of A549-ONG41008 interactome. By and large, the interactome study showed that FAS (a cell surface death receptor), NGFR (Neuronal Growth Factor Receptor), a death-domain containing cell surface receptor, and PGF (Placental Growth Factor) were linked to TRIAP1 (TP53 Regulated Inhibitor of Apoptosis 1) as an apoptosis nod of the interactome (Supplementary Figure 4). Furthermore, a TP53-regulated cell cycle hub was linked to the apoptosis hub through which CDKNIA also called

p21 was situated between these two interacting hubs. The TP3-regulated cell cycle hub comprised CEBPA, TP53INP1, BTG2, SSN1, SSN3, and HIST1H4K. Gene ontology was summarized in the pertinent boxes in Supplementary Figure 4. Interestingly, we noted that GDF15, a human TGFβ family member, may play an interesting role, probably in connecting two distinct systems and stabilizing them. GDF has been shown to be able to inter-connect two distinct biological systems [29].

Discussion

Fibrosis and cancer are still intractable and fatal diseases because fundamentals of these diseases are directly related to cell cycle regulation. Cell cycle control is meticulously regulated such that proliferation, differentiation or apoptosis should be harmonized. Dysfunction of this tight regulation may lead to vulnerability initiating serious diseases. Uncontrolled proliferation is the core of the vulnerability. The current anti-fibrotic and anti-cancer drugs are largely targeted to uncontrolled proliferation [30]. A number of side effects are associated with these drugs, leaving behind us regrets. Immune checkpoint inhibitors (ICIs) are becoming a very successful modality for dealing with cancer with much lesser side effects [31]. Immunity is able to distinguish self from non-self, conforming to *in vivo* cancer immunity. Here, we show that RS and OIS generated by ONG41008 were able to make DHLF and A549 liberated from uncontrolled proliferative status, respectively. Although we haven't tested many normal cells ONG41008, at least, was capable of clearly distinguishing pathogenic myofibroblasts from normal lung fibroblasts, giving a great surprise to us. When ONG41008 was orally administered into mice or rats no pathological abnormalities or toxicities were seen at 1g of ONG41008 (preclinical study number: U-18156), suggesting that ONG41008 is a safe drug for normal cell types.

Pathogenic myofibroblasts and cancer cells are in common such that metabolic features gaining ATP stem from aerobic glycolysis, resulting in dysregulated redox potential represented by NAD/NADH ratio. ATP levels or intracellular pH may become similar. Chromone scaffold (CS) is the core structure found in flavones or isoflavones [32], which has been known to capture UV in such a way that plants are protected from UV damage. Although over 10,000 kinds of CS-containing derivatives (CSD) have been discovered the number of

CSD exhibiting anti-fibrotic capacity seems to be limited, suggesting that not only CS but also a variety of side chains linked CS may contribute to anti-fibrosis. It has been reported that CS plays a role in anti-cancer activity; SB203580 [33]. Since ONG41008 is able to distinguish pathogenic myofibroblasts (DHLF) and cancer cells (A549) we would like propose that the CS of ONG41008 may be able to recognize some elements comprising intracellular micro-environments involving NAD, NADH, pH or ATP as an energy sensor. As ONG41008 was able to normalize NAD/NADH ratio in a range of 60 to 100 we speculate that the normalized NAD/NADH ratio may influence ROS production in the ONG41008-treated A549, thereby leading to OIS. Essentially, since ONG41008 is able to enhance NAD intracellular concentrations its rate-limiting enzyme, Nampt (Nicotinamide phosphoribosyltransferase), could be a primary target for ONG41008.

All thing considered, we believe that ONG41008 is a potent inducer of cellular senescence (RS and OIS) and pathogenic myofibroblasts or cancer cells can be liberated from their diseased uncontrolled proliferation loops.

Acknowledgments

We are thankful to all those Osteoneurogen researchers and administrative workforces who have been helping us, thereby making the current manuscript possible. We were indebted to Drs. JB Kim, I-H Kim, and HS Kim for their valuable advices. A special thanks would be given to Christine Youn encouraging this study to be evolved. This study was supported by an intramural fund from Osteoneurogen, Inc. (ONG-400021)

Competing financial interests

B-S Youn retain the shares of Osteoneurogen, M-K Meang retains a stock option, and SB Kim are employed by OsteoNeuroGen. The current contents of the ONG41008 data has been subjected to a Korean provisionary patent.

Author contributions

B-S Youn conceived the idea and wrote the manuscript. MK Maeng was largely involved in executing major experiments involving methods and materials. SB Kim played a major role in conducting drug responsiveness of DHLF and NHLF.

***Footnotes:**

The following abbreviated terms were mainly used in this manuscript;

CS: Chromone Scaffold

CSD: Chromone Scaffold Derivatives

DHLF: Diseased Human Lung Fibroblasts from IPF patients

NHLF: Normal Human Lung Fibroblasts

RS: Replicative Senescence

OIS: Oncogene-Induced Senescence

MNC: Multinucleation

MTMP: Mitochondrial Membrane Potential

NAD: nicotinamide adenine dinucleotide **NAMPT**: Nicotinamide Phosphoribosyltransferase

References

1. Wang JJ, Lei KF, Han F. Tumor microenvironment: recent advances in various cancer treatments. Eur Rev Med Pharmacol Sci 2018; 22: 3855-3864. DOI: 10.26355/eurrev_201806_15270
2. Maier D, Nagel AC, Preiss A. Two isoforms of the Notch antagonist Hairless are produced by differential translation initiation. Proc Natl Acad Sci U S A 2002; 99: 15480-15485. DOI: 10.1073/pnas.242596699
3. Gallorini M, Cataldi A, di Giacomo V. Cyclin-dependent kinase modulators and cancer therapy. BioDrugs 2012; 26: 377-391. DOI: 10.1007/bf03261895
4. Chen T, You Y, Jiang H et al. Epithelial-mesenchymal transition (EMT): A biological process in the development, stem cell differentiation, and tumorigenesis. J Cell Physiol 2017; 232: 3261-3272. DOI: 10.1002/jcp.25797
5. Nowell PC. The clonal evolution of tumor cell populations. Science 1976; 194: 23-28. DOI: 10.1126/science.959840
6. van Meerbeeck JP, Fennell DA, De Ruysscher DK. Small-cell lung cancer. Lancet 2011; 378: 1741-1755. DOI: 10.1016/s0140-6736(11)60165-7
7. Luengo A, Li Z, Gui DY et al. Increased demand for NAD(+) relative to ATP drives aerobic glycolysis. Mol Cell 2021; 81: 691-707.e696. DOI: 10.1016/j.molcel.2020.12.012
8. Pavlides S, Tsirigos A, Vera I et al. Transcriptional evidence for the "Reverse Warburg Effect" in human breast cancer tumor stroma and metastasis: similarities with oxidative stress, inflammation, Alzheimer's disease, and "Neuron-Glia Metabolic Coupling". Aging (Albany NY) 2010; 2: 185-199. DOI: 10.18632/aging.100134

9. Singh M, Kaur M, Silakari O. Flavones: an important scaffold for medicinal chemistry. Eur J Med Chem 2014; 84: 206-239. DOI: 10.1016/j.ejmech.2014.07.013

10. Fischer N, Seo EJ, Efferth T. Prevention from radiation damage by natural products. Phytomedicine 2018; 47: 192-200. DOI: 10.1016/j.phymed.2017.11.005

11. Quintão NLM, Pastor MVD, Antonialli CD et al. Aleurites moluccanus and its main active constituent, the flavonoid 2″-O-rhamnosylswertisin, in experimental model of rheumatoid arthritis. J Ethnopharmacol 2019; 235: 248-254. DOI: 10.1016/j.jep.2019.02.014

12. Lu QQ, Chen YM, Liu HR et al. Nitrogen-containing flavonoid and their analogs with diverse B-ring in acetylcholinesterase and butyrylcholinesterase inhibition. Drug Dev Res 2020. DOI: 10.1002/ddr.21726

13. Kim H-S, Meang MK, Ham M et al. Discovery of a small molecule having both potent anti-fibrotic and anti-inflammatory capabilities. bioRxiv 2020; 770404. DOI: 10.1101/770404

14. Richeldi L, du Bois RM, Raghu G et al. Efficacy and safety of nintedanib in idiopathic pulmonary fibrosis. N Engl J Med 2014; 370: 2071-2082. DOI: 10.1056/NEJMoa1402584

15. Lancaster LH, de Andrade JA, Zibrak JD et al. Pirfenidone safety and adverse event management in idiopathic pulmonary fibrosis. Eur Respir Rev 2017; 26. DOI: 10.1183/16000617.0057-2017

16. Goldmann T, Zissel G, Watz H et al. Human alveolar epithelial cells type II are capable of TGFβ-dependent epithelial-mesenchymal-transition and collagen-synthesis. Respir Res 2018; 19: 138. DOI: 10.1186/s12931-018-0841-9

17. Carvalho C, L'Hôte V, Courbeyrette R et al. Glucocorticoids delay RAF-induced senescence promoted by EGR1. J Cell Sci 2019; 132. DOI: 10.1242/jcs.230748

18. Huang J, Zhang J, Bellani MA et al. Remodeling of Interstrand Crosslink Proximal Replisomes Is Dependent on ATR, FANCM, and FANCD2. Cell Rep 2019; 27: 1794-1808.e1795. DOI: 10.1016/j.celrep.2019.04.032

19. Suhail TV, Singh P, Manna TK. Suppression of centrosome protein TACC3 induces G1 arrest and cell death through activation of p38-p53-p21 stress signaling pathway. Eur J Cell Biol 2015; 94: 90-100. DOI: 10.1016/j.ejcb.2014.12.001

20. Michowski W, Chick JM, Chu C et al. Cdk1 Controls Global Epigenetic Landscape in Embryonic Stem Cells. Mol Cell 2020; 78: 459-476.e413. DOI: 10.1016/j.molcel.2020.03.010

21. Senderowicz AM. Cell cycle modulators for the treatment of lung malignancies. Clin Lung Cancer 2003; 5: 158-168. DOI: 10.3816/CLC.2003.n.028

22. Yu M, Qi B, Xiaoxiang W et al. Baicalein increases cisplatin sensitivity of A549 lung adenocarcinoma cells via PI3K/Akt/NF-κB pathway. Biomed Pharmacother 2017; 90: 677-685. DOI: 10.1016/j.biopha.2017.04.001

23. Di Micco R, Fumagalli M, Cicalese A et al. Oncogene-induced senescence is a DNA damage response triggered by DNA hyper-replication. Nature 2006; 444: 638-642. DOI: 10.1038/nature05327

24. Rao G, Pierobon M, Kim IK et al. Inhibition of AKT1 signaling promotes invasion and metastasis of non-small cell lung cancer cells with K-RAS or EGFR mutations. Sci Rep 2017; 7: 7066. DOI: 10.1038/s41598-017-06128-9

25. Halazonetis TD, Gorgoulis VG, Bartek J. An oncogene-induced DNA damage model for cancer development. Science 2008; 319: 1352-1355. DOI: 10.1126/science.1140735

26. Chen J. The Cell-Cycle Arrest and Apoptotic Functions of p53 in Tumor Initiation and Progression. Cold Spring Harb Perspect Med 2016; 6: a026104. DOI: 10.1101/cshperspect.a026104

27. Buchakjian MR, Kornbluth S. The engine driving the ship: metabolic steering of cell proliferation and death. Nat Rev Mol Cell Biol 2010; 11: 715-727. DOI: 10.1038/nrm2972

28. Xie N, Zhang L, Gao W et al. NAD(+) metabolism: pathophysiologic mechanisms and therapeutic potential. Signal Transduct Target Ther 2020; 5: 227. DOI: 10.1038/s41392-020-00311-7

29. Luan HH, Wang A, Hilliard BK et al. GDF15 Is an Inflammation-Induced Central Mediator of Tissue Tolerance. Cell 2019; 178: 1231-1244.e1211. DOI: 10.1016/j.cell.2019.07.033

30. Evan GI, Vousden KH. Proliferation, cell cycle and apoptosis in cancer. Nature 2001; 411: 342-348. DOI: 10.1038/35077213

31. Schoenfeld AJ, Hellmann MD. Acquired Resistance to Immune Checkpoint Inhibitors. Cancer Cell 2020; 37: 443-455. DOI: 10.1016/j.ccell.2020.03.017

32. Reis J, Gaspar A, Milhazes N et al. Chromone as a Privileged Scaffold in Drug Discovery: Recent Advances. J Med Chem 2017; 60: 7941-7957. DOI: 10.1021/acs.jmedchem.6b01720

33. Yan W, Xiaoli L, Guoliang A et al. SB203580 inhibits epithelial-mesenchymal transition and pulmonary fibrosis in a rat silicosis model. Toxicol Lett 2016; 259: 28-34. DOI: 10.1016/j.toxlet.2016.07.591

Figure legends

Figure 1. Comparison of survival rate of DHLF and NHLF treated with ONG41008, Nintedanib, or Pirfenidone A-B) DHLF (Diseased Human Lung Fibroblasts) and NHLF (Normal Human Lung Fibroblasts) were stimulated in the absence of TGFβ with various concentrations of the drugs as indicated up to 30μM for 24hr, 48hr and 72hr. Cell survival rate was measured by CCK-8. IC50 of Nintedanib was calculated within Sigmoidal, Fourth Party Logistics by GraphPad Prism 7.00.

Figure 2. No apoptotic effects on the induction of the ONG41008-mediated growth arrest of DHLF DHLF were collected and re-seeded into each culture dishes pertinent to corresponding apoptotic assays; A) Activated caspase3 assay was performed using ONG41008, Nintedanib, or Pirfenidone. B) Mitochondrial membrane potentials were measured. FCCP was used as a control being a mitochondrial oxidative phosphorylation uncoupler. C) Lactate dehydrogenase (LDH) was assayed. IC_{50} or EC_{50} was measured at 72hr with Sigmoidal, Fourth Party Logistics by GraphPad Prism 7.00.

Figure 3. Induction of RS by ONG41008 and an interactome analysis A) DHLF were treated with different concentrations of ONG41008 along with control (RPMI medium). Immunocytochemistry (ICC) was conducted with anti-human GATA6, phalloidin, and DAPI. Morphological change was monitored under phase contrast microscopy. Typical replicative senescent cells were denoted by “replicative senescence” white-colored. B) An RNA-seq

analysis was conducted using total RNAs prepared from non-treated DHLF or 10μM ONG41008-treated DHLF. An interactome representing upregulated genes was established via the String program based upon p-values (>0.005).

Figure 4. Translocation of TP53 to the nuclei and both induction and nuclear translocation of p21 and p16 in DHLF upon ONG41008 treatment DHLF were treated with 1μM to 10μM ONG41008 along with control (RPMI medium). ICC were conducted with anti-human TP53, anti-p21, anti-p16, or phalloidin in conjunction with DAPI; A) Translocation of p53 to the nuclei was demonstrated. B-C) Induction and translocation of p21 and p16 to the nuclei were shown, respectively.

Figure 5. Capability of ONG41008 with respect to induction of a robust cellular senescence leading to multinucleation A549 were stimulated with 10μM ONG41008 for 24hr, 48hr, or 72hr and subjected to ICC by using anti-ZEB1, DAPI, and Phalloidin; A) ICC for ONG41008-treated A549 at 24hr was conducted in which flat cells representing MNC denoted with white circles along with control presented. B-C) ICCs for ONG41008-treated A549 at 48hr and 72hr were conducted, respectively. MNC were also denoted by white circles.

Figure 6. Translocation of TP53 to the nuclei, and both induction and nuclear translocation of p21, and both induction and perinuclear and nuclear translocation of p16 in A549 upon ONG41008 treatment A-C) A549 were stimulated with varying concentrations of ONG41008, 1μM to 20μM, and ICC was conducted with anti-TP53, anti-

p21, or anti-p16. D) A549 were treated with 10μM ONG41008 for 72hr during which control and ONG41008 was everyday replaced with new media and new batch of 10μM ONG41008, respectively. p16 expression was detected by ICC.

Figure 7. Western blot analysis of TP53, p21, and p16 and microscopic observation of cell death of A549 A) Cell lysates were prepared from A549 treated with different concentrations, 1μM to 50μM for 24hr and subjected to western blot using pertinent antibodies as indicated. Yellow circles represent respective molecular mass. B) A549 were continually treated with 20μM ONG41008 for 15 days in the presence of TGFβ (2.5ng/ml) in order to keep cells vibrant along with control A549. Cell death was monitored under phase contrast microscopy.

Figure 8. Induction of cellular senescence of human aggressive cancer cells upon ONG41008 treatment A549, MCF7, or PANC1 was stimulated with 20μM ONG41008 for 24hr. ICC was conducted with the use of Phalloidin and DAPI and merged imaging was compared.

Figure 9. Comparison of anti-cancer capabilities associated with ONG41008 with SAHA and Nintedanib in A549 and their toxic effects on NHLF. A) Survival rates of A549 treated with ONG41008 or SAHA were measured via CCK-8. IC50s were measured. B) NHLF were stimulated with ONG41008, SAHA or Nintedanib for various time points as indicated. CCK-8 assays were conducted. C and D) NHLF were stimulated with ONG41008, SAHA or Nintedanib. MTMP and LDH were measured, respectively. IC50s were measured.

Figure 10. **ONG41008-mediated G2/M cell cycle arrest and massive induction of NAD/NADH** A) A549 were stimulated with ONG41008 for 24hr or 48hr and subjected to PI staining. Acquisitions of cell cycle analyses were conducted by FACS. B) A549 were stimulated with medium alone, varying concentrations of SAHA or ONG41008 for 24hr. Cell lysates were prepared and subjected to calculation of NAD/NADH ratio.

Figure 11. A working hypothesis on RS in DHLF and OIS of in A549 induced by ONG41008 While ONG41008 was responsible for inducing replicative senescence in DHLF it was able to induce OIS followed by multinucleation, which caused apoptosis of A549. Regardless of both cell types participation of TP53, p21, and p16 is required for both types of senescence occurred in DHLF and A549. ONG41008 does not affect induction of TP53. Translocation of TP53, p21, and p16 is necessary for cell cycle arrest.

Materials and Methods

Cell culture and reagents

DHLFs were purchased from Lonza (Basel, Switzerland) and cultured in fibroblast growth medium (FBM, Lonza, Walkersville, MD, USA). Recombinant human TGFβ and PDGF were obtained from Peprotech (Rocky Hill, CT, USA) and used at a final concentration of 5 ng/ml. Chemically synthesized ONG41008 was obtained from Syngene International Ltd. (Bangalore, India), dissolved at a stock concentration of 50 mM in DMSO, and stored in aliquots at -20°C. DMSO with according concentration was used as control. RAW264.7 cell line was purchased from Korean Cell Line Bank (Seoul, Korea) and cultured in RPMI supplemented with 10% FBS and 1% P/S (Welgene, Seoul, Korea). LPS was purchased from Sigma and used at final concentration of 100 ng/ml.

Immunocytochemistry

Cells were fixed using 4% paraformaldehyde, permeabilized with 0.4% TritonX100, blocked with 1% BSA and incubated with Rhodamine Phalloidin(Thermo Fisher, Massachusetts, USA), anti-GATA6(Abcam, Cambridge, UK), Anti-p53(Cell signaling technology, Beverly, MA), p21(Abcam, Cambridge, UK), p16-INK4A(Proteintech, IL, USA), ZEB1(Cell signaling technology, Beverly, MA) for 4 hour at RT. After washing, cells were incubated with Alexa Fluor 488(Abcam, Cambridge, UK) conjugated secondary antibody. Images were analyzed using EVOS M7000(Invitrogen, CA, USA)

Western Blot

A549 cells were seeded at 1 × 10^6cells/well in 100mm cell culture dishes and incubated overnight, followed by treatment with various concentrations of ONG41008. After 24 hr, The cell lysates were clarified by centrifugation at 14,000 x g for 10 minutes and the supernatant was collected. The protein concentrations were quantified by Bradford assay (Thermo Fisher, Massachusetts, USA). Thereafter, 25ug of cellular protein was loaded on 10% SDS-PAGE gel and transferred to Nitrocellulose membranes. After blocking with 5% BSA, the membranes were incubated with Anti-p53(Cell signaling technology, Beverly, MA), phosphor-p53(Cell signaling technology, Beverly, MA), p21(Abcam, Cambridge, UK), p16-INK4A (Proteintech, IL, USA), GAPDH (Abcam, Cambridge, UK) overnight at 4'C. after washing thoroughly, membranes were incubated with HRP-conjugated secondary antibody. Protein band was visualized using ECL reagent (Abfrontier, Korea) and Uvitec HD9(UVITEC, UK)

Live Imaging

DHLFs were seeded at 12 well cell culture plates, and after 24hr, TGF beta (5ng/ml), Nintedanib (10uM), Pirfenidone (10uM) and ONG41008 (10uM) were treated. Cells were incubated in EVOS M7000 CO^2 incubation chamber (Invitrogen, CA, USA), cell morphology images were captured every 30 minutes. The snapshots were collected and attached as dynamic video.

CCK-8 assays

Cells were seeded onto 96well plates at a density of 3×10^4cell/well for 24hr. Then the cells were treated with 0.01, 0.1, 1, 10, 20, 30uM ONG41008 or Pirfenidone or Nintedanib. After

treatment, cell survival rate was measured by cell counting kit-8 (Dojindo, CK04) as manufacturer's protocol.

Caspase-3 assay

The caspase-3 activity was measured using Caspase-3 assay kit (abcam, ab37401). Cells treated with various concentrations of ONG41008 or Pirfenidone or Nintedanib were harvested and lysed on ice. Thereafter, protein was measured by BCA (Thermo, 23227) and adjusted to 50ug protein per 50ul cell lysis buffer. Then the caspase-3 activity was examined by following manufacturer's protocol.

Mitochondrial Membrane Potential assay

Cells were seeded in 96 wells plate for 24hr, then exposed to different concentration of ONG41008 or Prifenidone or Nintedanib. The cells were then co-incubated with TMRE (abcam, ab113852), for 30min 37℃ in the dark. Cells treated 20uM FCCP were used as positive control. After that, mitochondrial membrane potential was examined by following manufacturer's protocol.

LDH assay

LDH release were detected by using the LDH assay kit (abcam, ab56393). The cell culture plates were centrifuged at 480g for 10min, and supernatants (10ul/well) were extracted into another 96well plate. Then, 100ul LDG reaction mix was added to each well and incubation

for 30min at room temperature. The absorbance values were measured at 450nm on the microplate reader.

NAD/NADH assay

Total NAD was extracted and quantified from A549 cell lysates using the NAD+/NADH Colorimetric Assay Kit (Abcam, ab65348) following the manufacturer's instructions. 1×10^6cells were lysed in 400ul NAD/NADH extraction buffer, filtered through a 10 kD Spin Column (ab93349) and measured neat or at 1/5 dilution. Briefly, the amount of total NAD was calculated from a standard curve (pmol) divided by the sample volume added to the reaction well (µl) and multiplied by the dilution factor.

RNA-seq processing, differential gene expression analysis, and interactome analysis

Processed reads were mapped to the *Mus musculus* reference genome (Ensembl 77) using Tophat and Cufflink with default parameters. Differential analysis was performed using Cuffdiff using default parameters. Further, FPKM values from Cuffdiff were normalized and quantitated using the R Package Tag Count Comparison (TCC) to determine statistical significance (e.g., P values) and differential expression (e.g., fold changes). Gene expression values were plotted in various ways (i.e., Scatter, MA, and Volcano plots), using fold-change values, using an R script developed in-house. The protein interaction transfer procedure was performed using the STRING database with the differentially expressed genes. A 60 Gb sequence was generated, and 10,020 transcripts were read and compared. The highest-confidence interaction score (0.9) was applied from the *Mus musculus* species, and information

about interacts were obtained based on text mining, experiments, and databases (http://www.string-db.org/). Due to company information sake the above detailed RNA-Seq or interactome data interpretation would be limited but essential data sufficiently supporting our assertion were provided.

Reverse transcriptase PCR and real-time PCR

Cells cultured in either 12 or 24-well plates were washed twice with cold PBS and harvested using TaKaRa MiniBEST Universal RNA extraction kit (Takara, Japan). RNA was purified using the same kit according to manufacturer's protocol. RNA was reverse-transcribed using the cDNA Synthesis Kit (PCRBio Systems, London, UK). Synthesized cDNA was amplified with StepOne Plus (Applied Biosystems, Life Technologies) and 2× qPCRBio Probe Mix Hi-ROX (PCRBio). Comparisons between mRNA levels were performed using the ΔΔCt method, with GAPDH as the internal control.

Supplemental information

Suppl. Video demonstration I: A 72hr-long video photographing at high DHLF cell density was conducted.

Suppl. Video demonstration II: A 72hr-long video photographing at low DHLF cell density was conducted.

Suppl. Table I: Top replicative senescence-initiating genes: soluble factors / receptors. An RNA-seq analysis was conducted with the use of total RNAs prepared from DHLF or ONG41008-treated DHLF for 24hr. Top twenty genes showing $p>0.005$ were selected.

Suppl. Figure 1 and Figure 2: An RNA-Seq was performed as described above. The genes were sorted out in such a way that three sets of genes showing their p-values were corresponding to between 0.005 and 0.05, or between 0.05 and 0.5 were selected and selected genes were further analyzed via the String Program, giving rise to three interactomes.

Suppl. Figure 3. Phospho-AKT expression pattern of A549 treated with ONG41008. A549 were stimulated with increasing concentrations of ONG41008 (1mM to 20mM). ICC was performed using anti-phospho-specific Akt1 and Phalloidin

Suppl. Figure 4. NMC formation of a human aggressive prostate cancer cell line PC3 by ONG41008 PC3 were cultured in RPMI and stimulated with 20μM ONG41008 for 24hr. Senescent cells were stained with Phalloidin and DAPI. NMC were indicated by white circles.

Suppl. Figure 5. A549-ONG41008 network An A549-ONG41008 interactome was established. An RNA-seq analysis was conducted with the use of total RNAs prepared from A549 or ONG41008-treated 549 for 24hr. Top twelve upregulated genes showing $p>0.005$ were selected and their interactome was established via the String Program.

A)

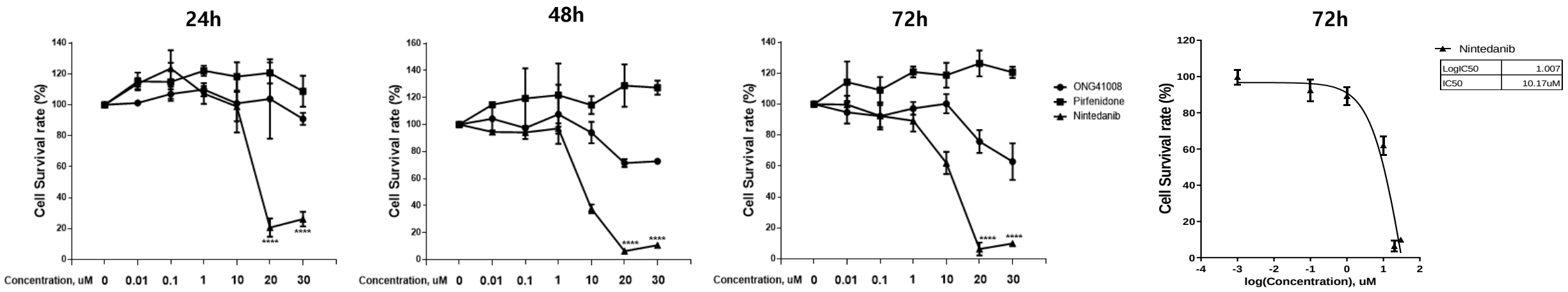
DHLF
24h
48h
72h
72h
Cell Survival rate (%)
Concentration, uM 0 0.01 0.1 1 10 20 30
ONG41008
Pirfenidone
Nintedanib
log(Concentration), uM
Nintedanib
LogIC50 1.007
IC50 10.17uM

B)

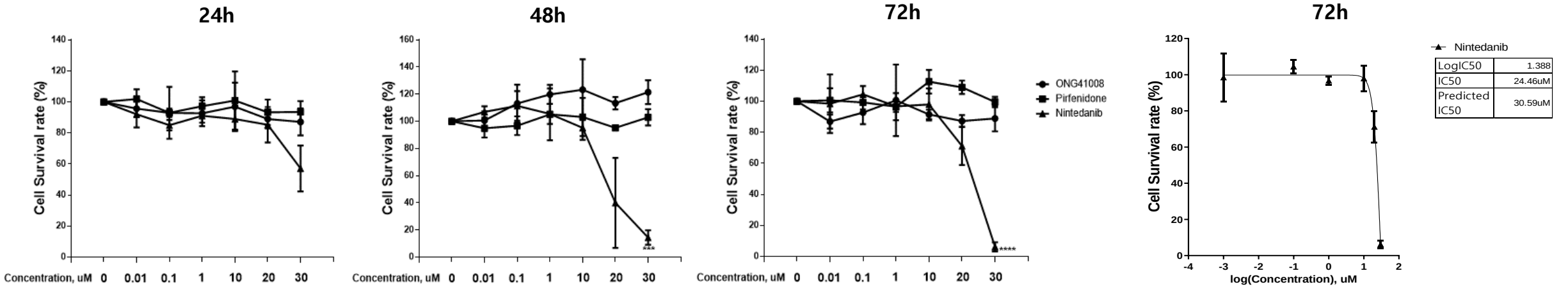
NHLF
24h
48h
72h
72h
Cell Survival rate (%)
Concentration, uM 0 0.01 0.1 1 10 20 30
ONG41008
Pirfenidone
Nintedanib
log(Concentration), uM
Nintedanib
LogIC50 1.388
IC50 24.46uM
Predicted IC50 30.59uM

Figure 1

Figure 2

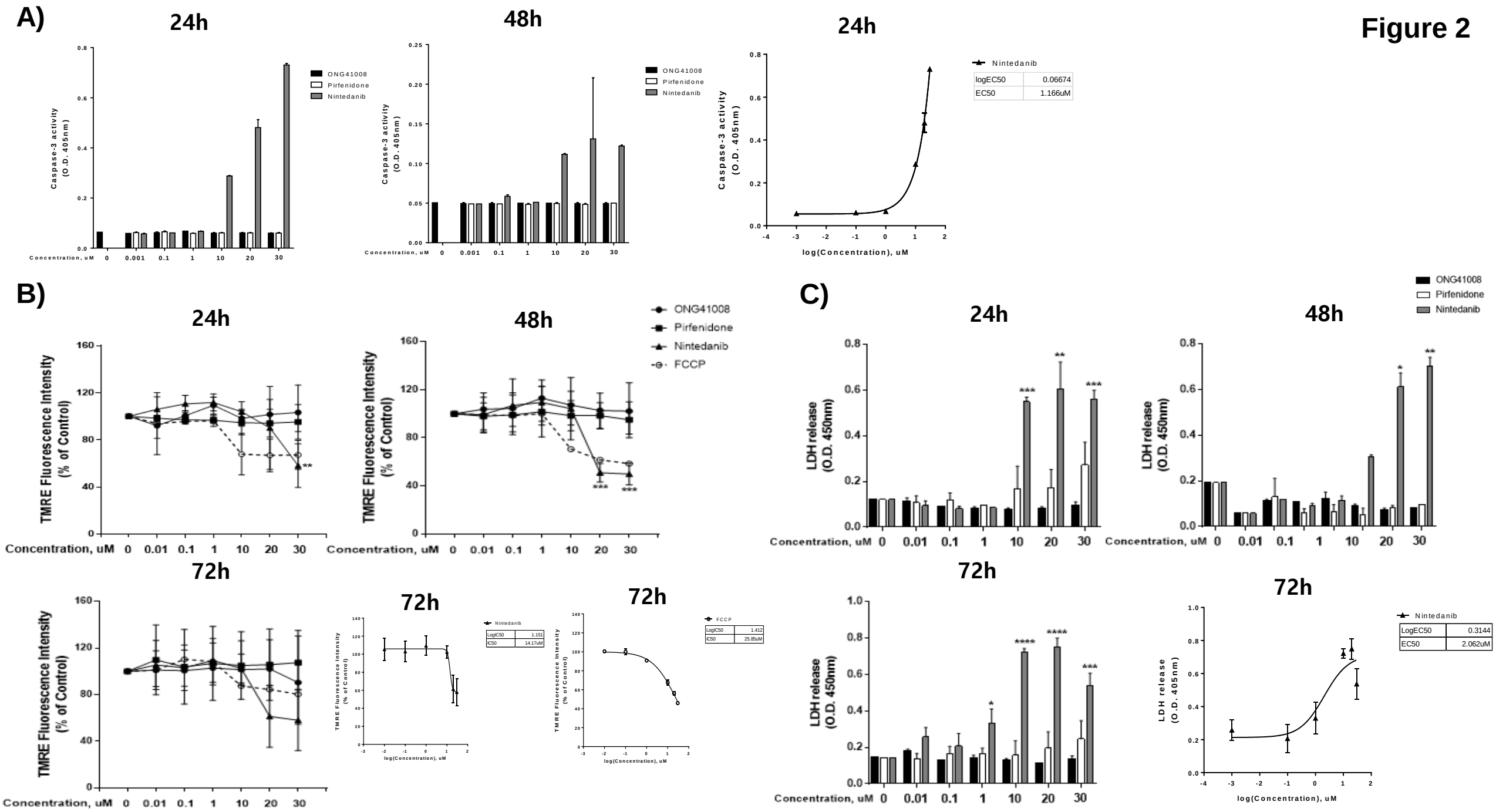
A)
24h
48h
24h
ONG41008
Pirfenidone
Nintedanib
Caspase-3 activity (O.D. 405nm)
Concentration, uM 0 0.001 0.1 1 10 20 30
log(Concentration), uM
Nintedanib
logEC50 0.06674
EC50 1.166uM
B)
24h
48h
ONG41008
Pirfenidone
Nintedanib
FCCP
TMRE Fluorescence Intensity (% of Control)
Concentration, uM 0 0.01 0.1 1 10 20 30
72h
72h
72h
Nintedanib
LogIC50 1.151
IC50 14.17uM
FCCP
LogIC50 1.412
IC50 25.85uM
log(Concentration), uM
C)
24h
48h
ONG41008
Pirfenidone
Nintedanib
LDH release (O.D. 450nm)
Concentration, uM 0 0.01 0.1 1 10 20 30
72h
72h
LDH release (O.D. 405nm)
Nintedanib
LogEC50 0.3144
EC50 2.062uM
log(Concentration), uM

A)

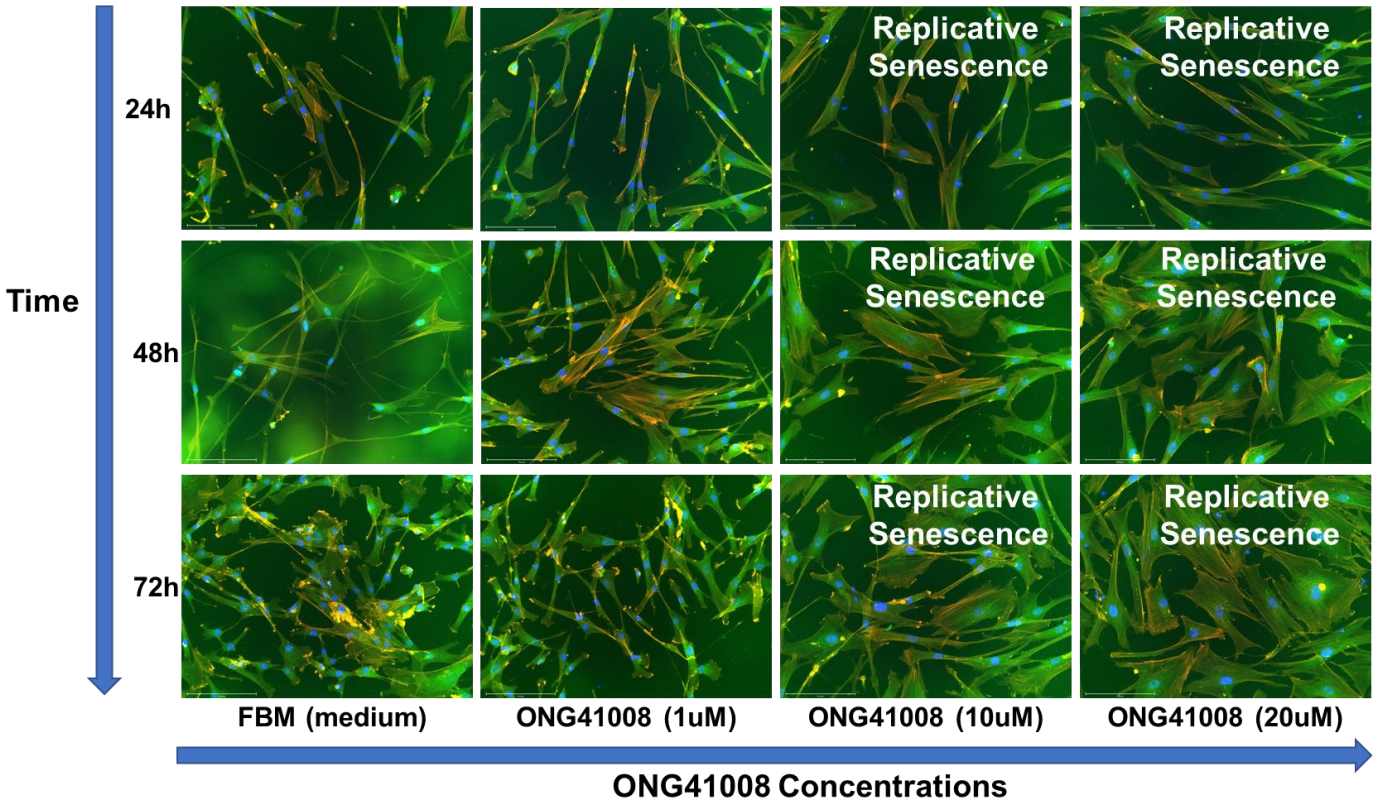
Time
24h
48h
72h
Replicative Senescence
FBM (medium)
ONG41008 (1uM)
ONG41008 (10uM)
ONG41008 (20uM)
ONG41008 Concentrations

B)

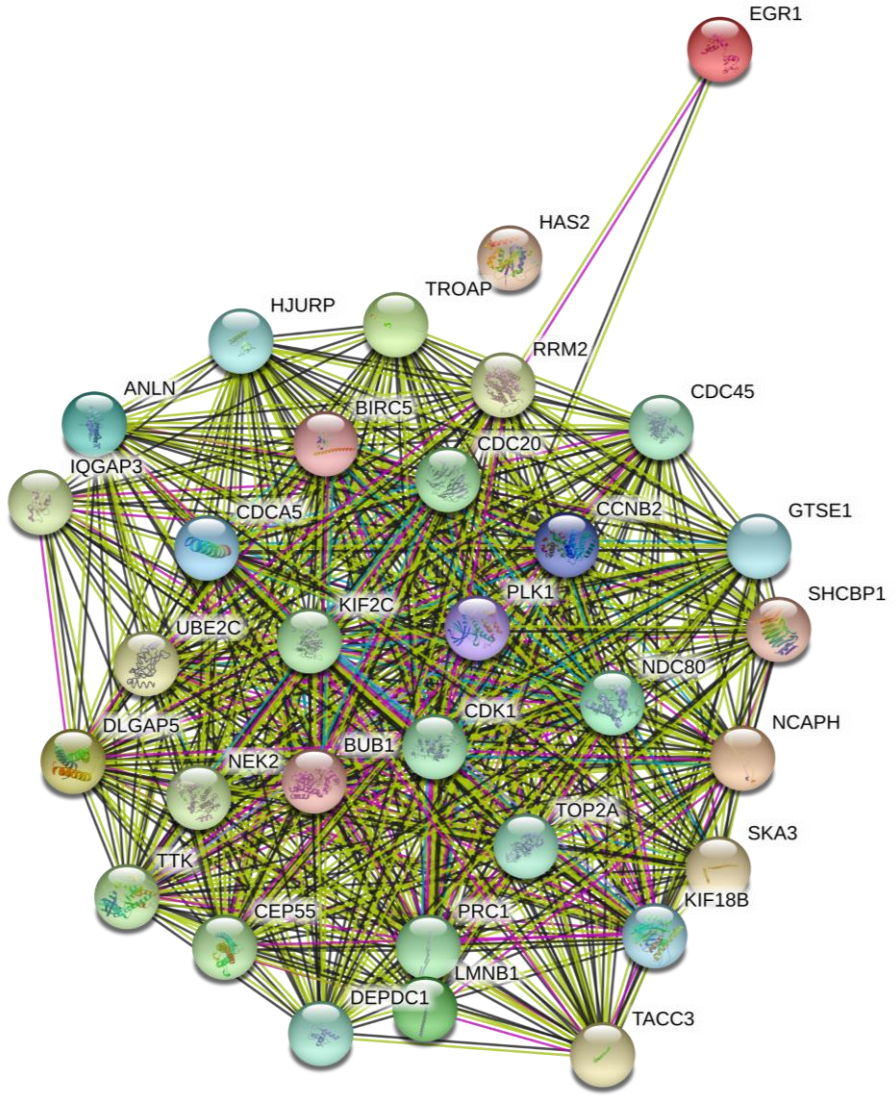
EGR1
HAS2
TROAP
HJURP
RRM2
ANLN
BIRC5
CDC45
CDC20
IQGAP3
CDCA5
CCNB2
GTSE1
PLK1
SHCBP1
KIF2C
UBE2C
NDC80
CDK1
NCAPH
DLGAP5
BUB1
NEK2
TOP2A
SKA3
TTK
KIF18B
CEP55
PRC1
LMNB1
DEPDC1
TACC3

Figure 3

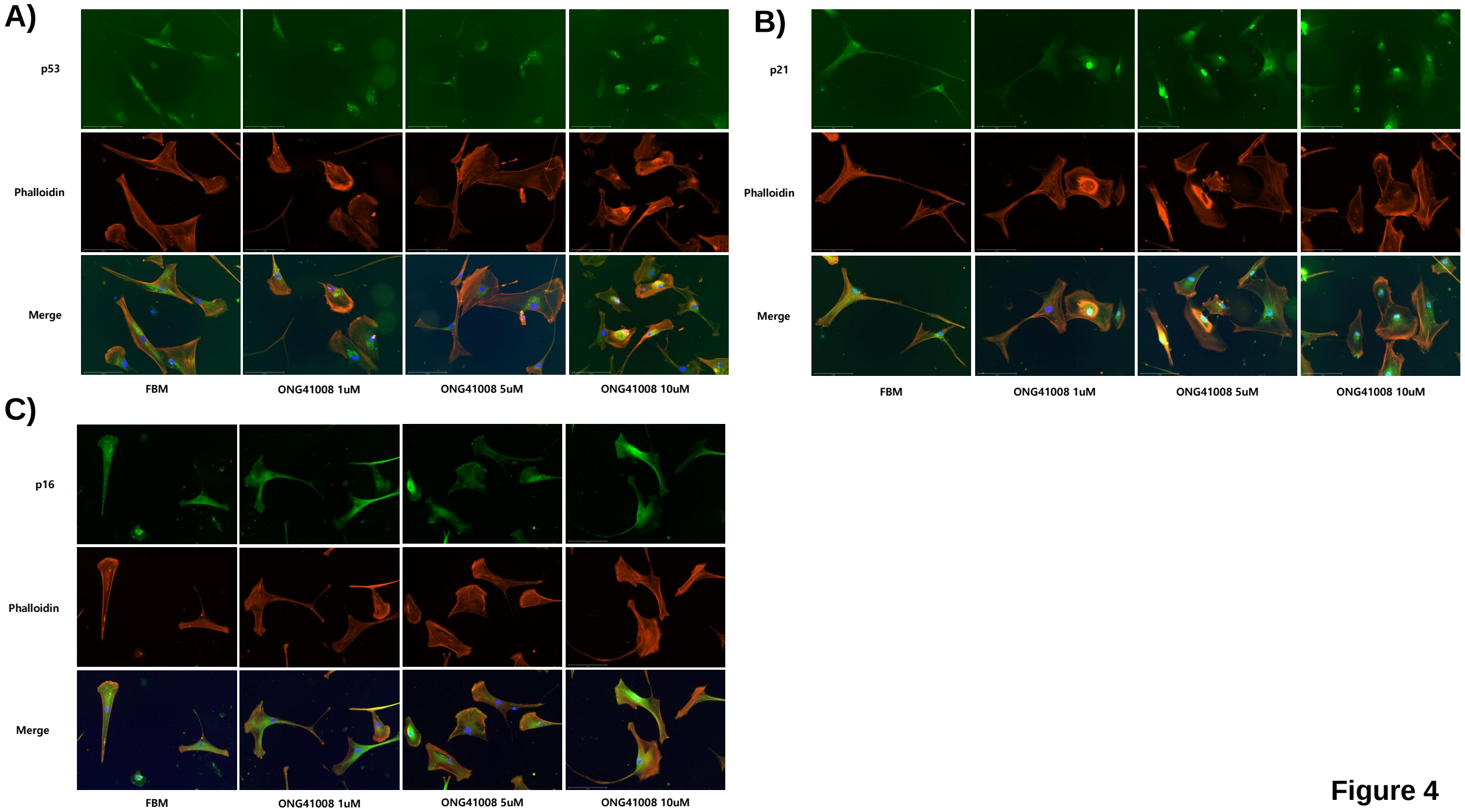
A)
p53
Phalloidin
Merge
FBM
ONG41008 1uM
ONG41008 5uM
ONG41008 10uM
B)
p21
Phalloidin
Merge
FBM
ONG41008 1uM
ONG41008 5uM
ONG41008 10uM
C)
p16
Phalloidin
Merge
FBM
ONG41008 1uM
ONG41008 5uM
ONG41008 10uM

Figure 4

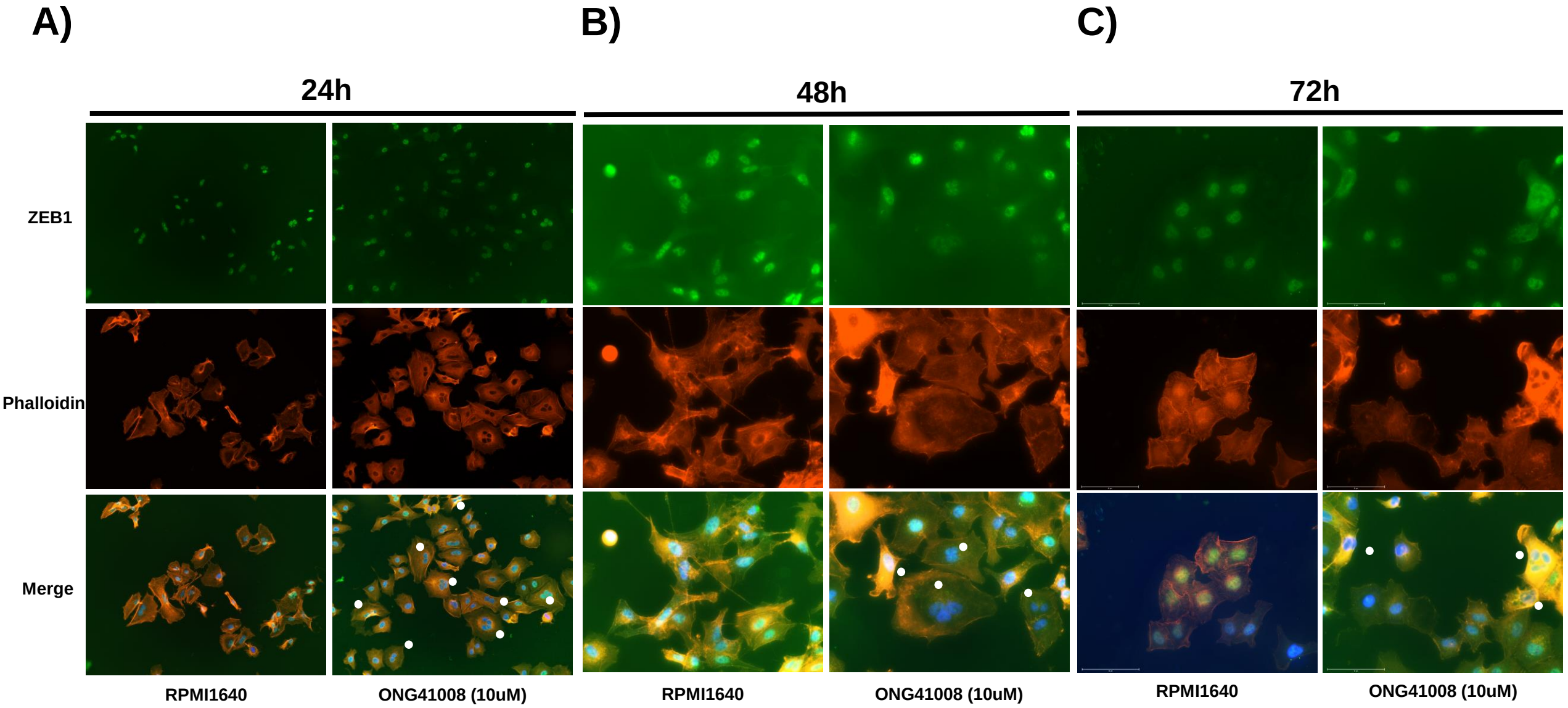
A)
B)
C)
24h
48h
72h
ZEB1
Phalloidin
Merge
RPMI1640
ONG41008 (10uM)
RPMI1640
ONG41008 (10uM)
RPMI1640
ONG41008 (10uM)

Figure 5

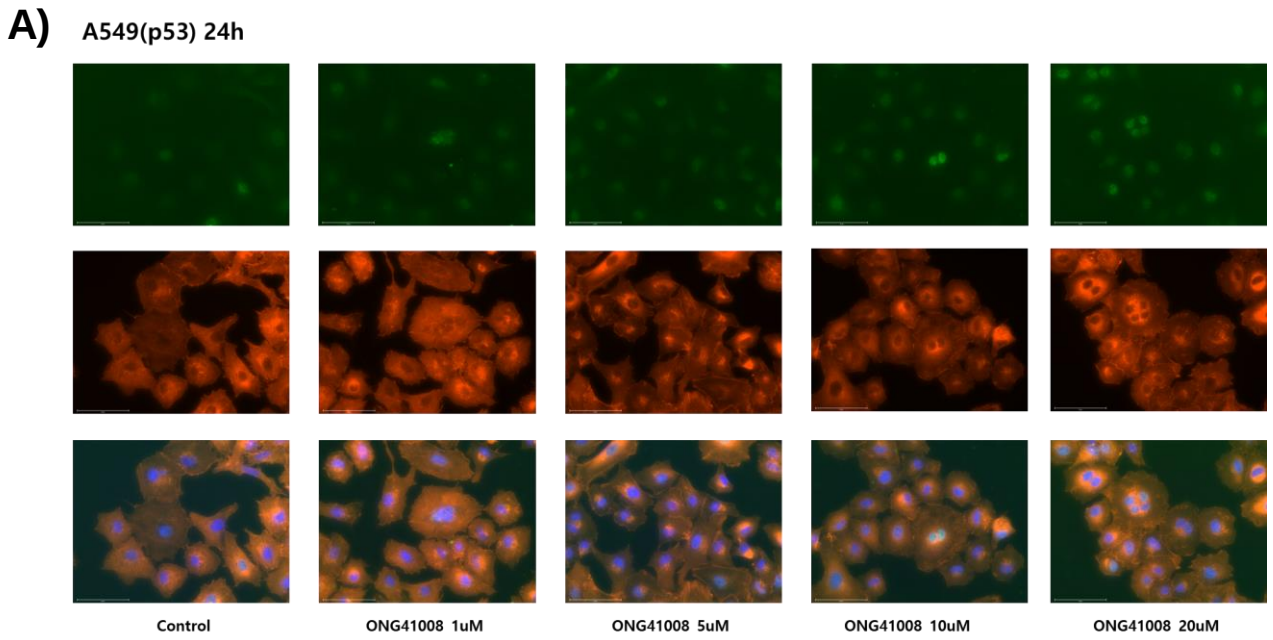
A)
A549(p53) 24h
Control
ONG41008 1uM
ONG41008 5uM
ONG41008 10uM
ONG41008 20uM

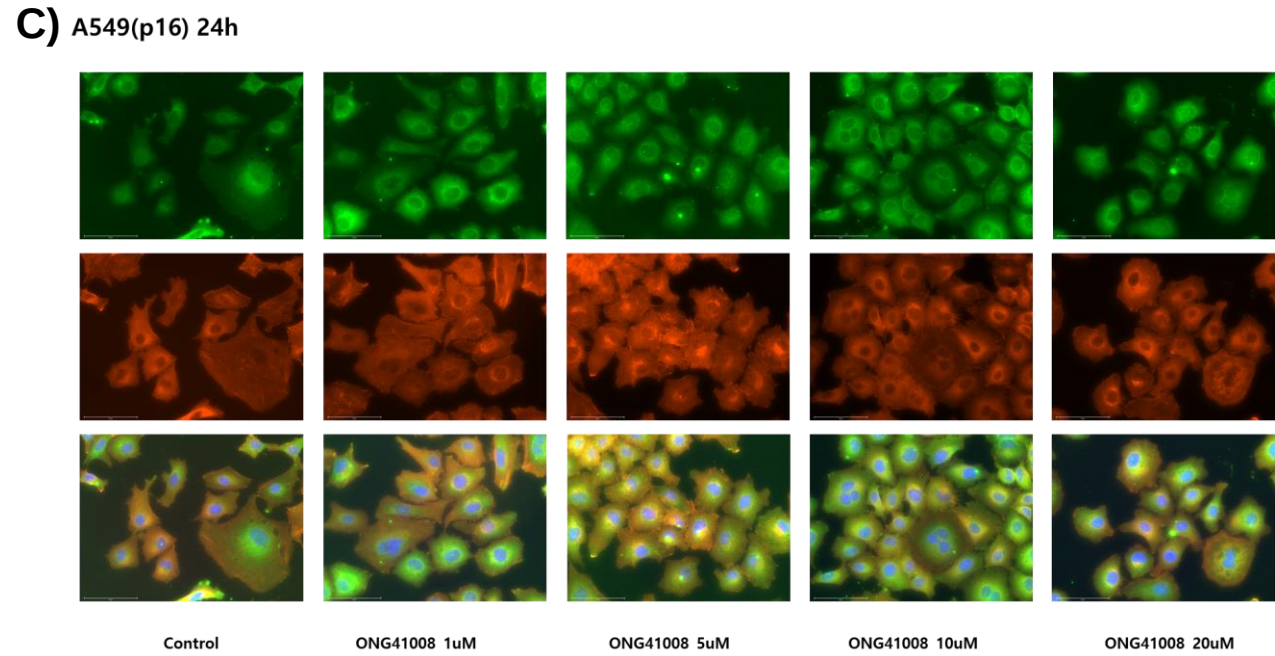
C)
A549(p16) 24h
Control
ONG41008 1uM
ONG41008 5uM
ONG41008 10uM
ONG41008 20uM

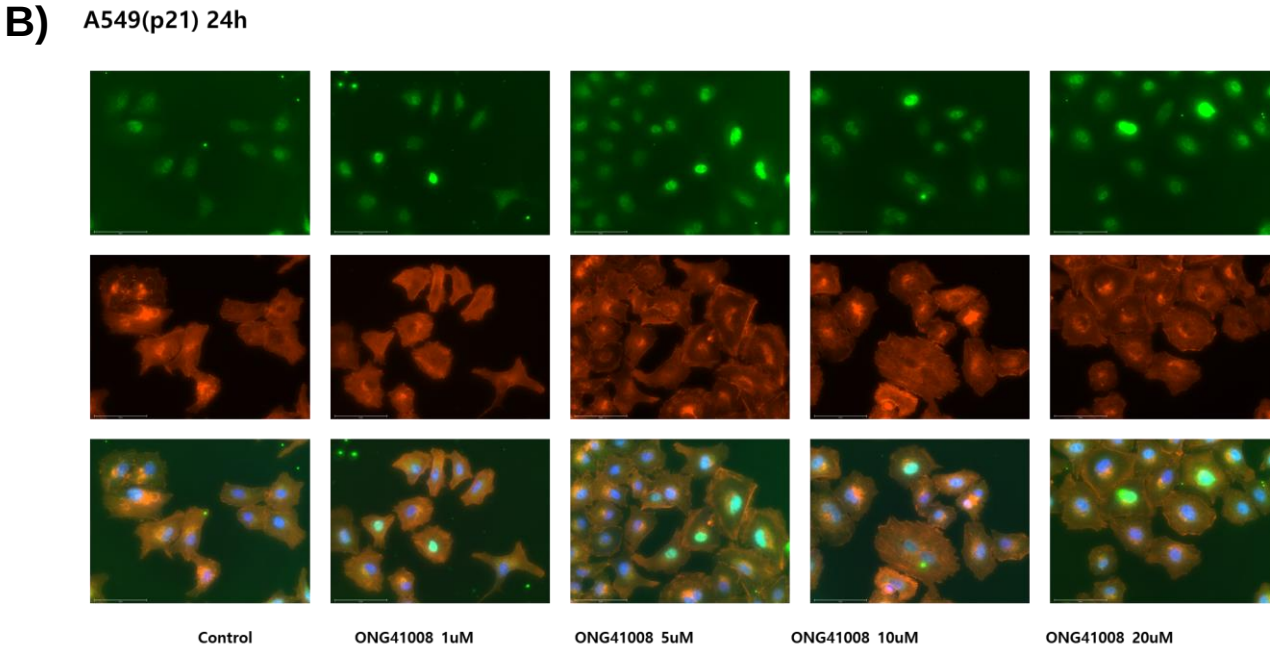
B)
A549(p21) 24h
Control
ONG41008 1uM
ONG41008 5uM
ONG41008 10uM
ONG41008 20uM

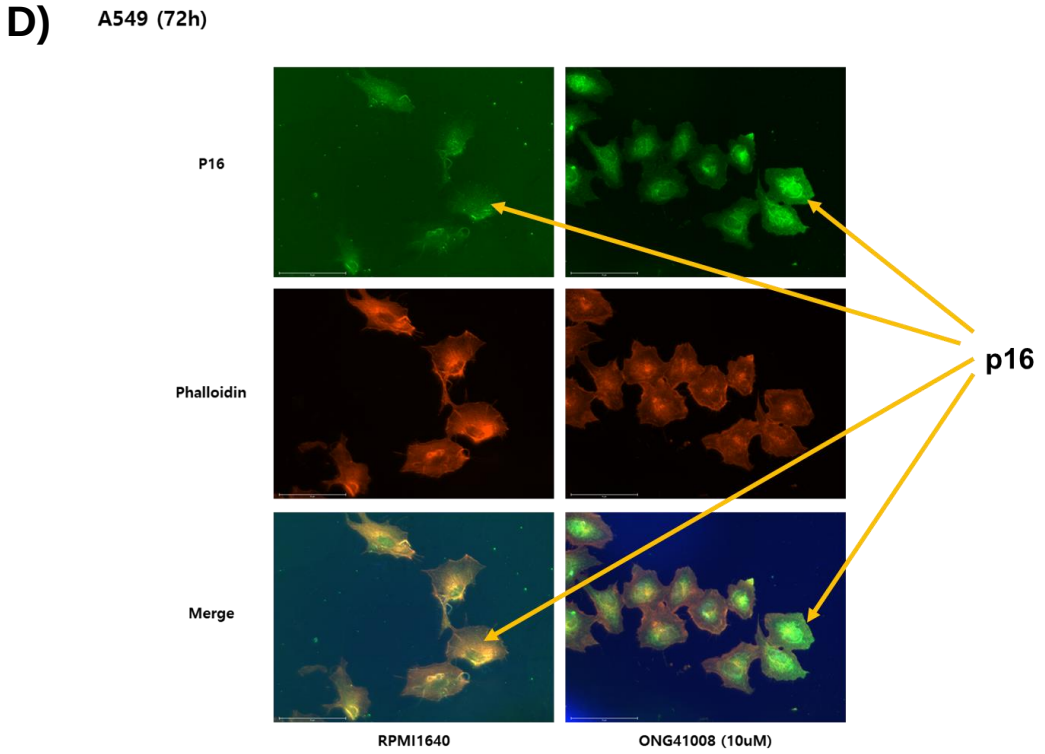
D)
A549 (72h)
P16
Phalloidin
Merge
p16
RPMI1640
ONG41008 (10uM)

Figure 6

A)

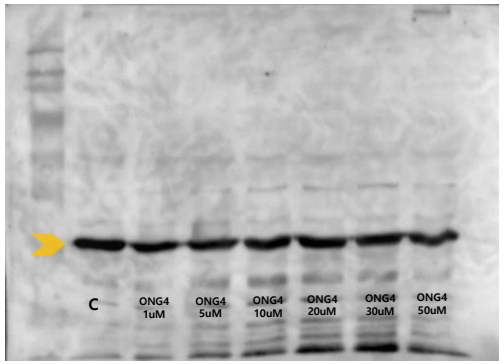

GAPDH

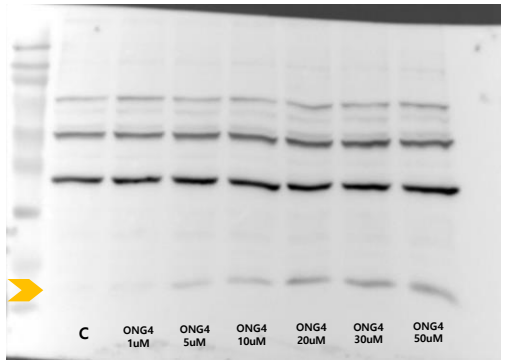

p21

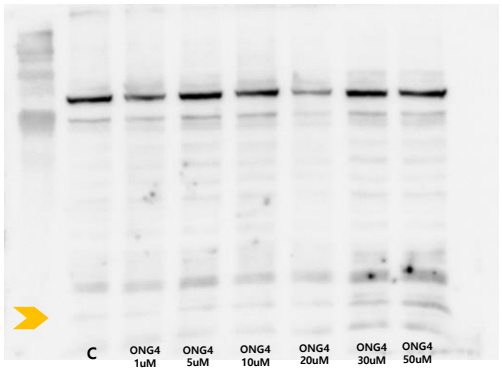

p16

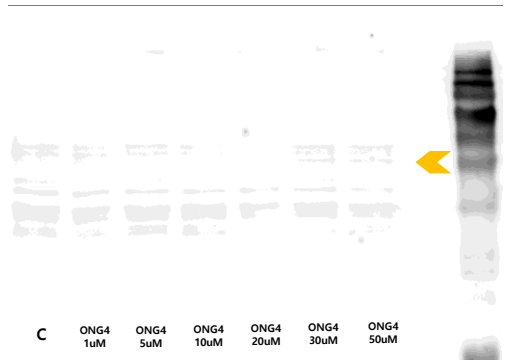

p53

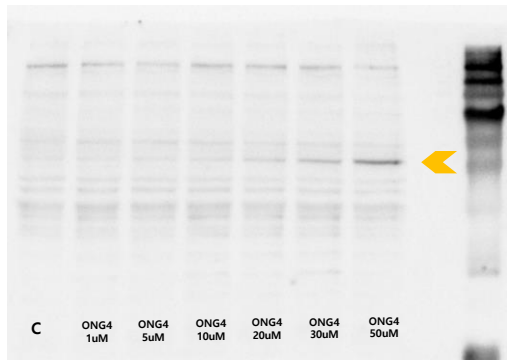

p-p53

B)

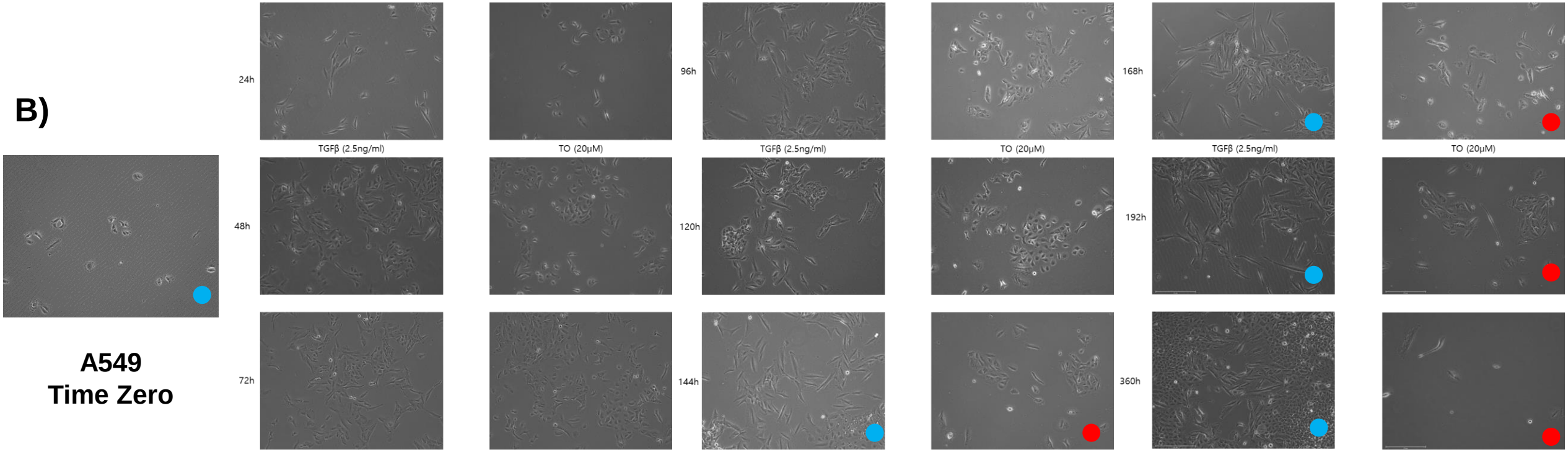

A549
Time Zero

TGFβ

TGFβ
+ ONG41008

TGFβ

TGFβ
+ ONG41008

TGFβ

TGFβ
+ ONG41008

Figure 7

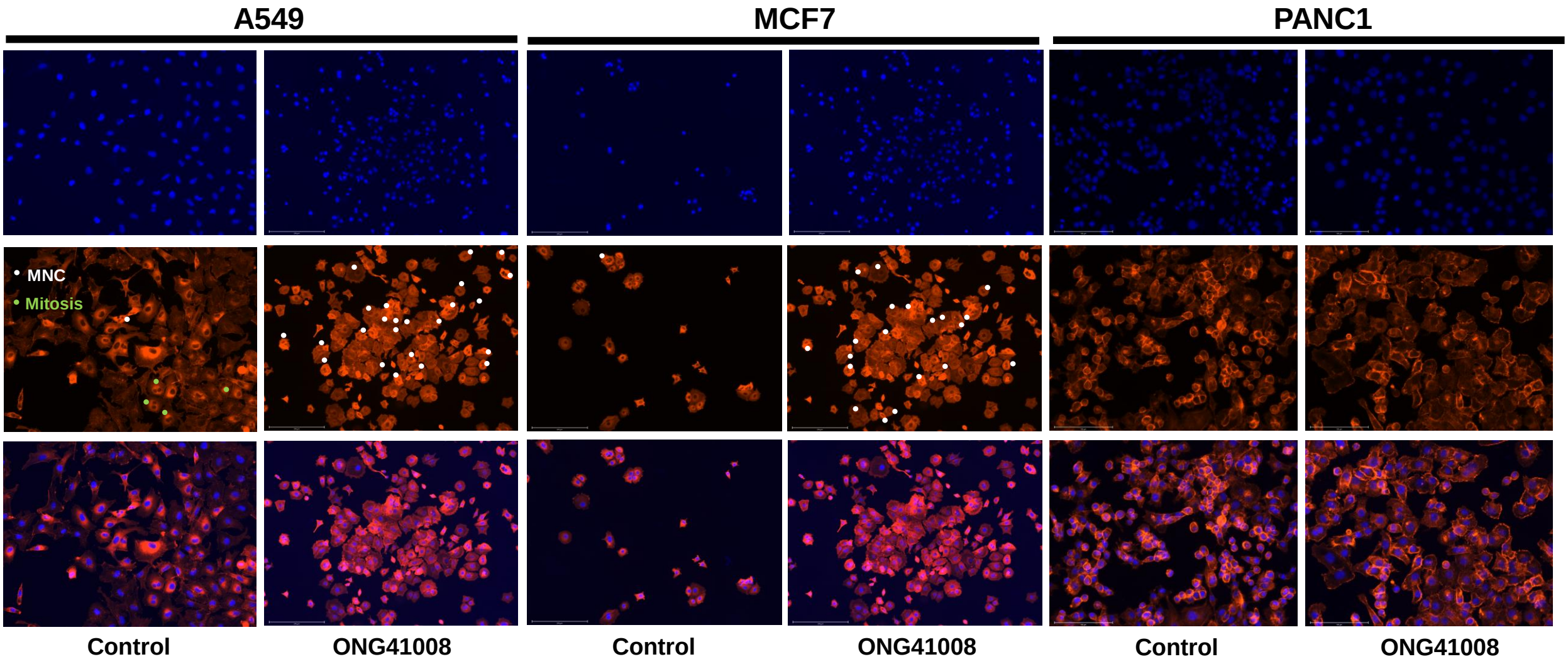
A549
MCF7
PANC1
MNC
Mitosis
Control
ONG41008
Control
ONG41008
Control
ONG41008

Figure 8

A)

A549

MTMP

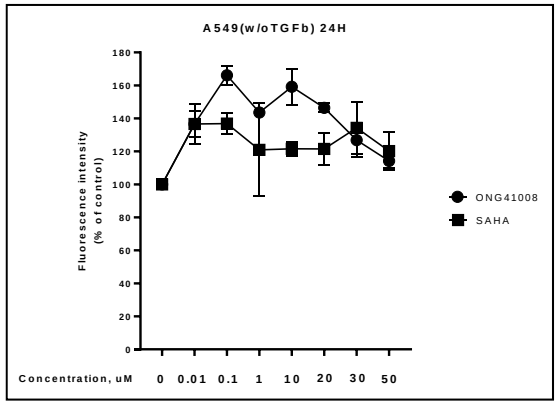

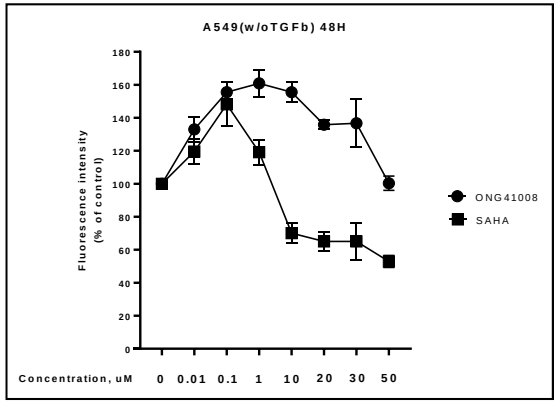

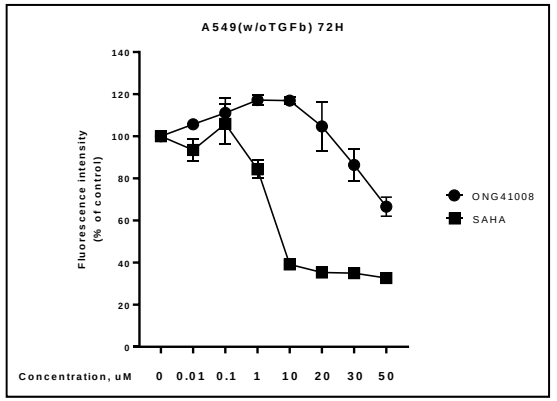

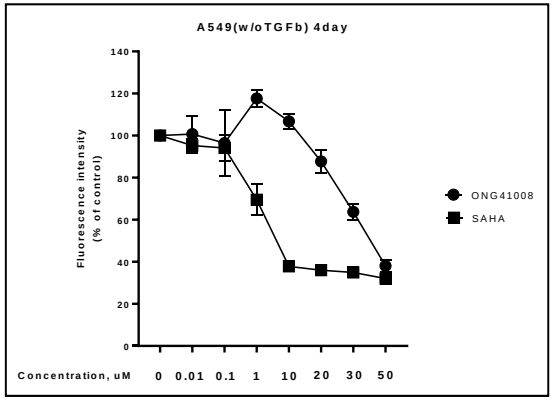

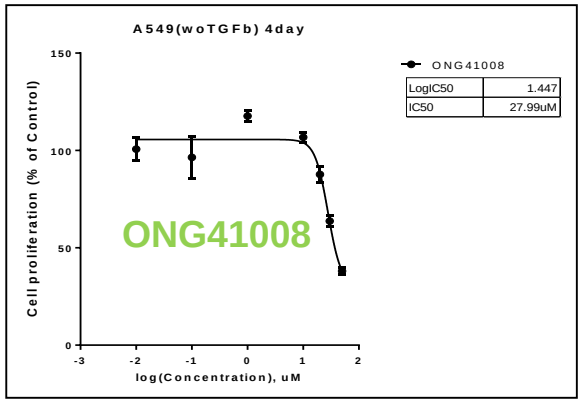

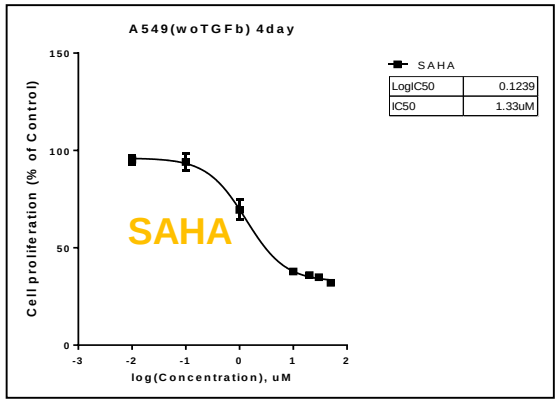

B)

NHLF

CCK-8

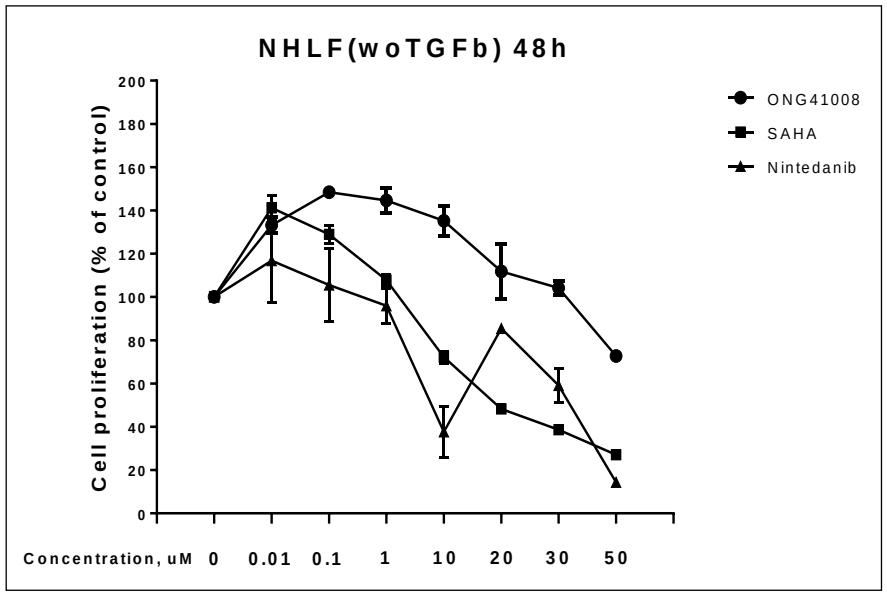

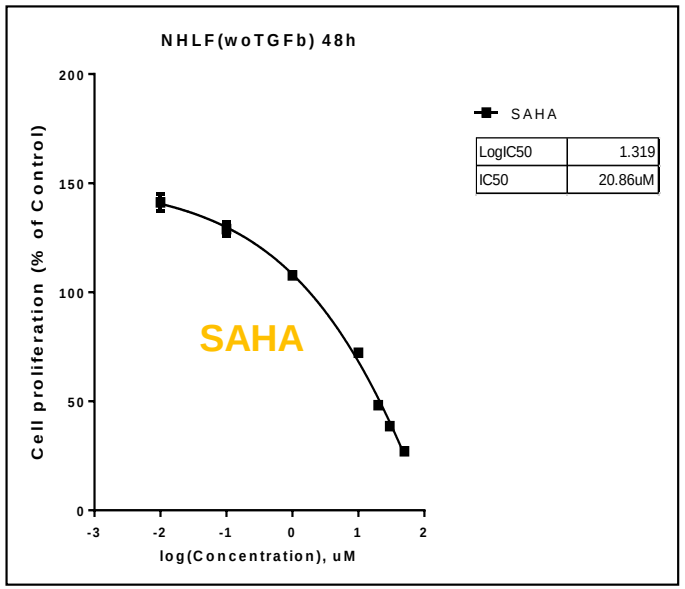

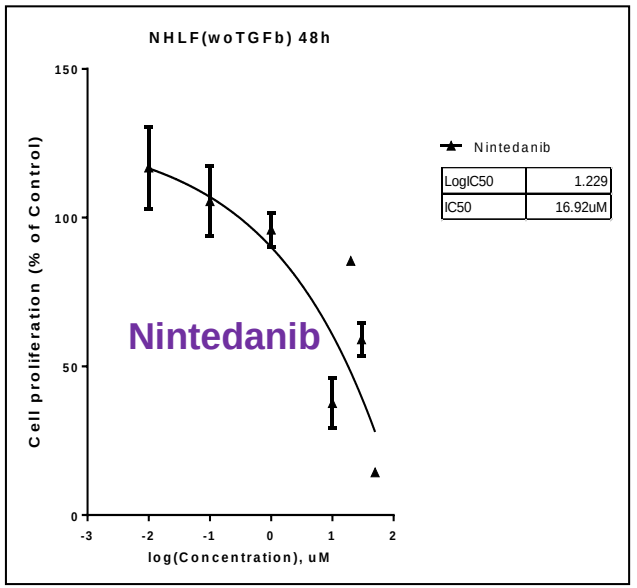

Figure 9

Figure 9

C)

NHLF

MTMP

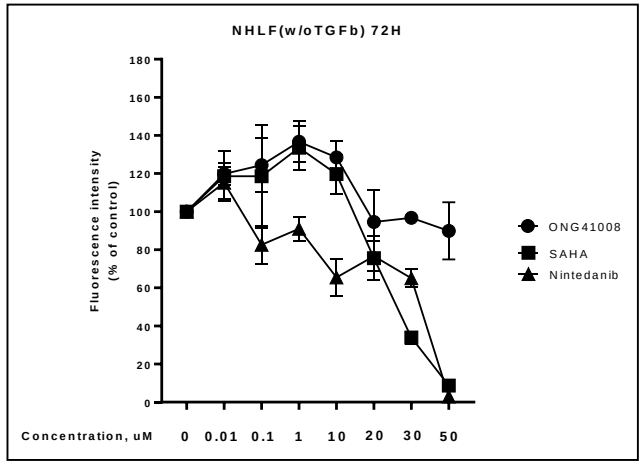

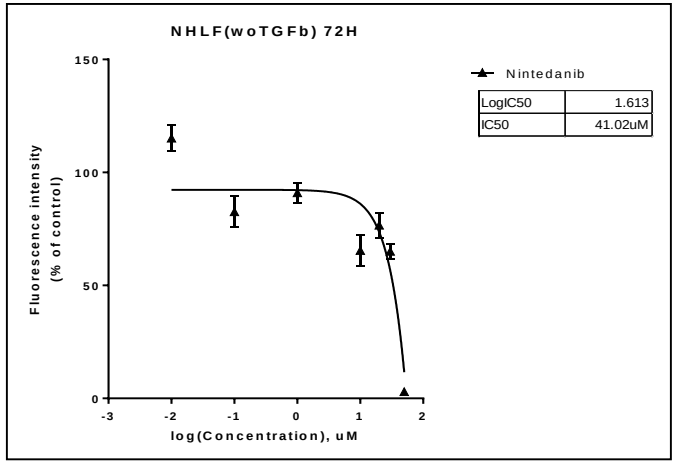

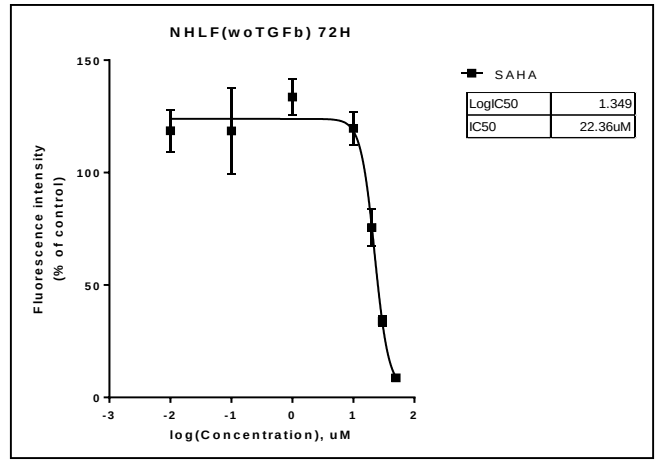

D)

NHLF

Caspase3

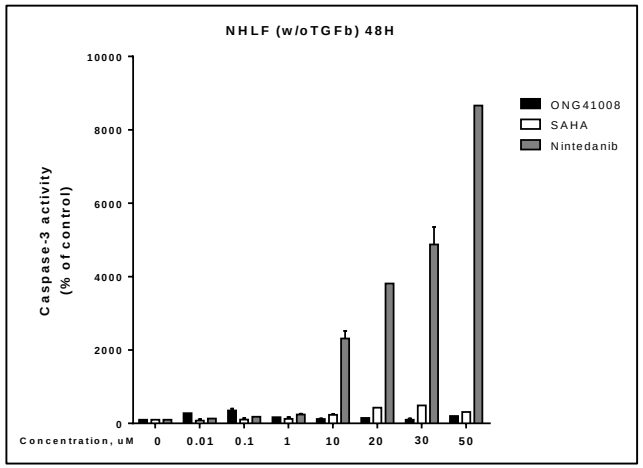

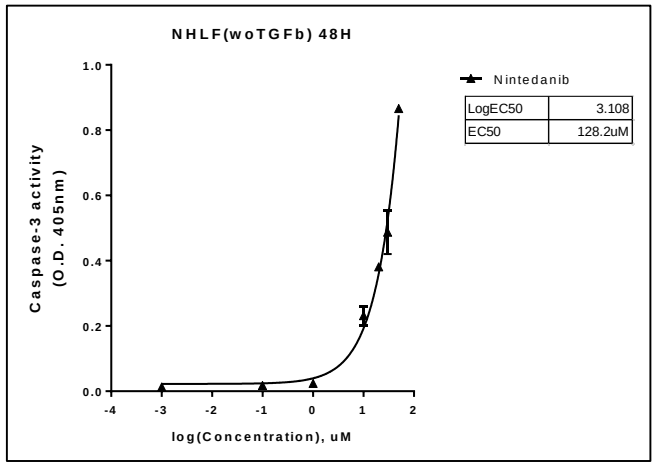

E)

NHLF

LDH

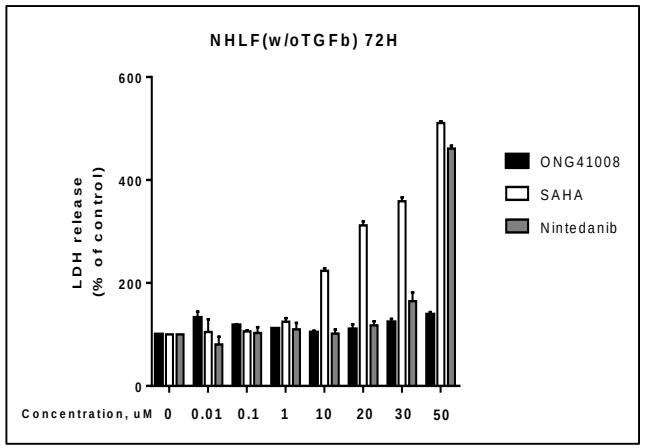

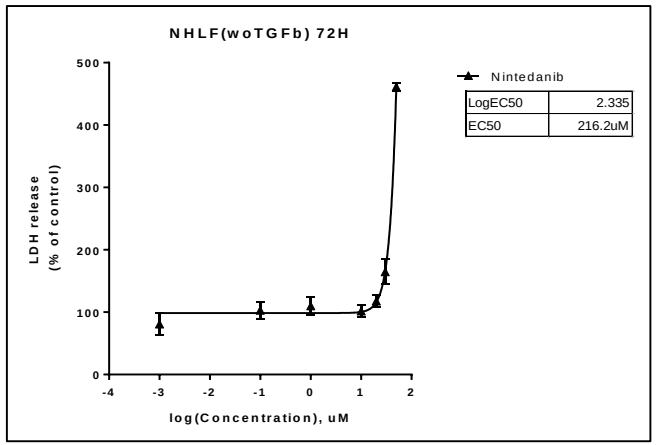

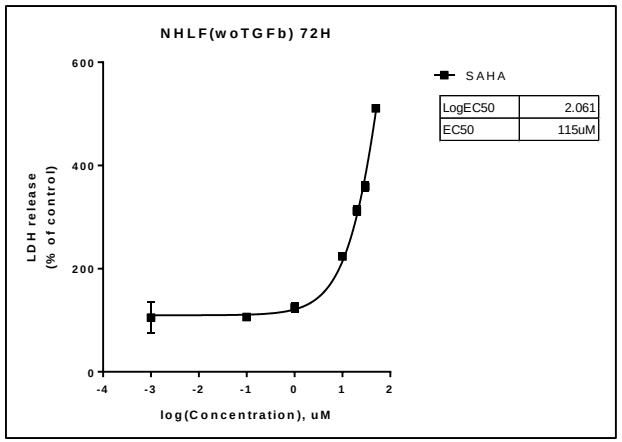

A)

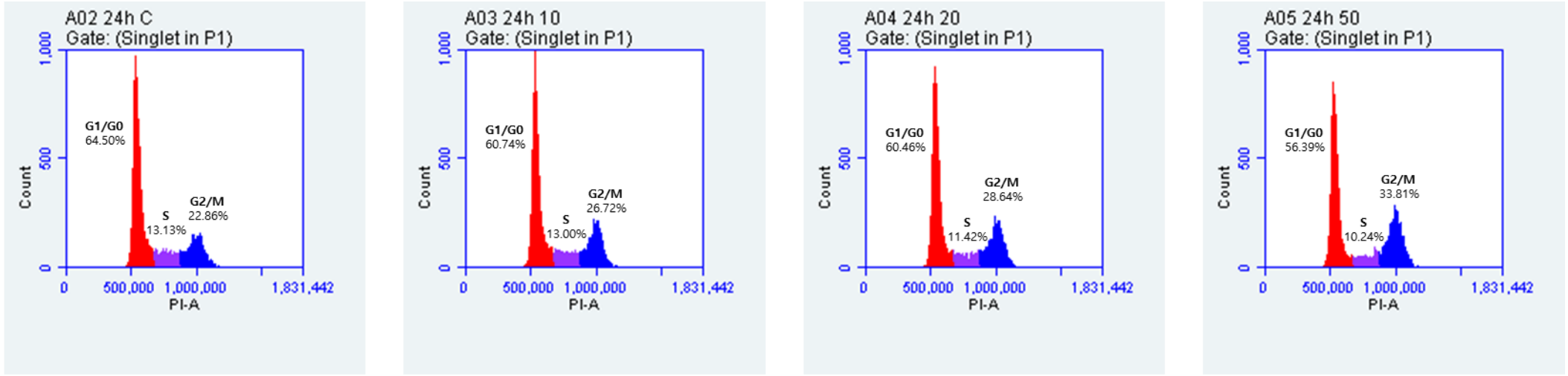

Control | ONG41008 10uM | ONG41008 20uM | ONG41008 50uM

B)

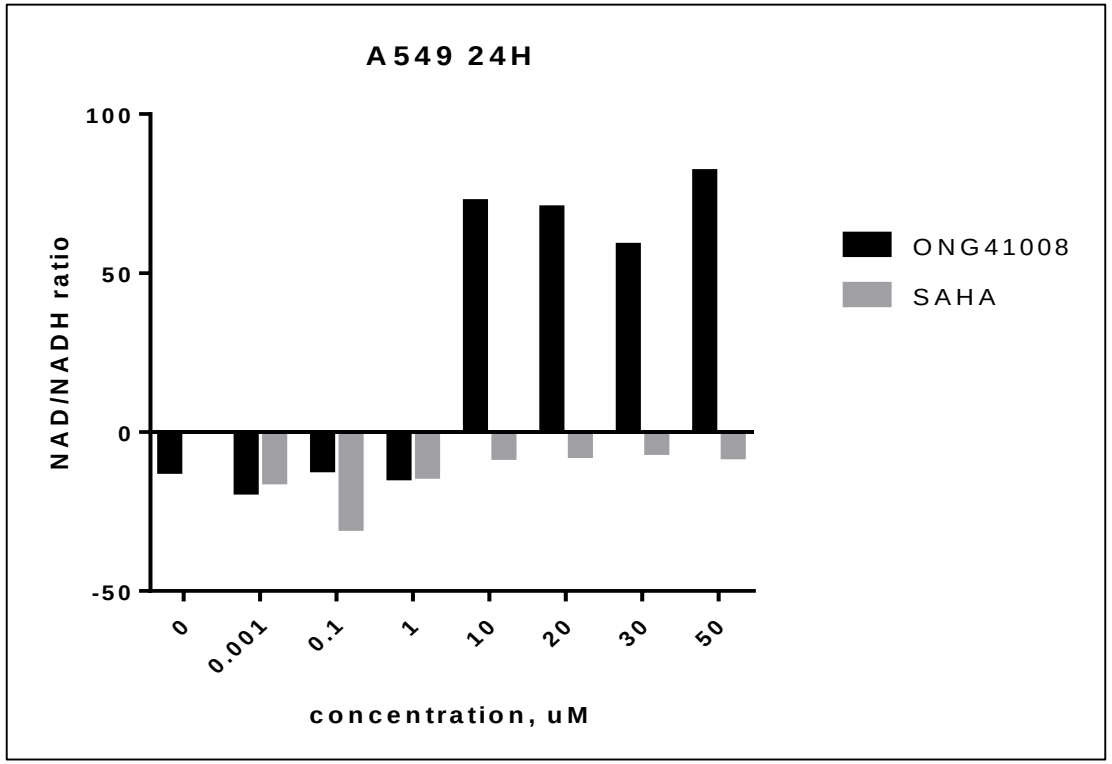

Figure 10

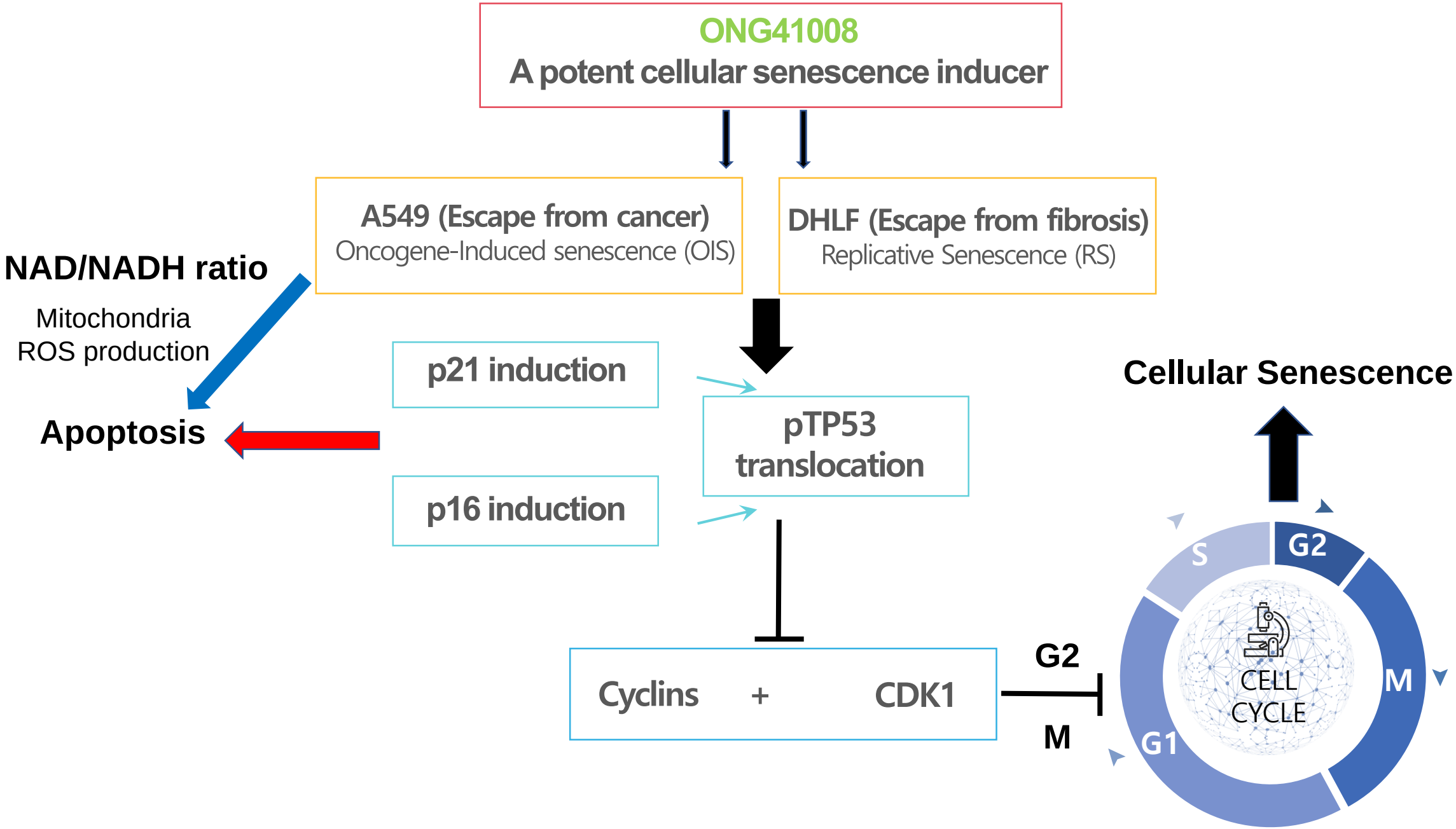
ONG41008
A potent cellular senescence inducer
A549 (Escape from cancer)
Oncogene-Induced senescence (OIS)
DHLF (Escape from fibrosis)
Replicative Senescence (RS)
NAD/NADH ratio
Mitochondria
ROS production
Apoptosis
p21 induction
p16 induction
pTP53
translocation
Cellular Senescence
Cyclins + CDK1
G2
M
S
G2
M
G1
CELL
CYCLE

Figure 11